Detonations in C_2H_4-O_2.

Experimental Measurements and Validation of Numerical Simulation for Incident and Reflected Waves.

Z. Liang, J. Karnesky and J. E. Shepherd
Graduate Aeronautical Laboratories

R. Deiterding
Center for Advanced Computing Research

California Institute of Technology
Pasadena, CA 91125

Explosion Dynamics Laboratory Report FM2006.009

June 25, 2008

Sponsored by the US DOE, NNSA through the Caltech ASC Alliance Program, Center for Simulation of Dynamic Response of Materials.

Abstract

Experiments were carried out in a closed tube to obtain measurements of incident and reflected pressure histories for detonations in stoichiometric ethylene-oxygen mixtures. The data are compared with the Chapman-Jouguet and Taylor-Zeldovich ideal model and also numerical simulations of the Euler equations. Detonation waves are observed to propagation within 1% of the Chapman-Jouguet velocity and the pressure history is slightly lower (8%) than the predicted ideal behavior. Reasonable agreement between experiment and numerical simulation of the Euler equations is found for incident waves and reflected waves close to the reflecting end of the tube. The disagreement is larger for reflected waves far from the reflecting end. Possible reasons for this disagreement are discussed.

Contents

List of Figures

List of Tables

1 Introduction

Experiments on detonation and coupling of detonation waves to structural response of confining metal tubes has been sponsored at Caltech as part of the Center for Simulation of Dynamic Response of Materials. This center is part of the Academic Strategic Alliance Program of the NNSA's Advanced Simulation and Computing (ASC) program. A series of experiments (Chao and Shepherd, 2005a, 2004, Chao, 2004, Chao and Shepherd, 2005b) and corresponding simulations (Deiterding et al., 2006a,b, Cirak et al., 2006, Deiterding et al., 2007) have been performed to examine the coupling between detonations and structural response in thin-wall tubes. These studies build on earlier work in our laboratory on elastic vibrations excited by shock (Beltman et al., 1999) and detonation waves (Beltman and Shepherd, 2002, 1998) inside tubes. We have examined excitation of elastic vibrations, detonation-driven fracture, detonation diffraction through a fixed-slot, and detonation diffraction through a variable slot created by plastic deformation of a portion of the tube surface. The studies on elastic vibrations, and diffraction through fixed and variable slots is described in a companion report by Shepherd et al. (2008).

This report documents experimental tests performed in 2005 and 2006 to provide benchmark experimental data on two situations. First, we measured the pressure histories and extracted arrival time and the peak pressure for incident detonation and reflected shock waves. The motivation for these experiments was to resolve discrepancies between observed and predicted values that appeared to be a consequence of systematic differences in actual and documented experimental configurations. This data was also used to create model pressure profiles for simulations of elastic wave generation used in validation studies described in Shepherd et al. (2008). Second, we developed a new experimental configuration with venting through slots or movable flaps. This configuration was designed specifically for providing validation data for fluid-structure simulations and to be more repeatable than the fracturing tube configuration.

2 Experimental Configuration

The test facility was based on the precision test rig that is described in Chao (2004). This consists of a main detonation tube coupled to a test specimen tube (Fig. 1). The detonation is initiated and stabilized in the main tube, which is a 6.35 mm wall thickness, 1.607 m long aluminum tube. A stoichiometric ethylene-oxygen mixture (C_2H_4+$3O_2$) was ignited by an electrical spark at the end of the main detonation tube, and a Schelkin spiral was used to accelerate the flame into a detonation. The spiral consisted of a 10-in length of spring welded to a tubular insert. After propagating out of the main tube, the detonation entered a 6061-T6 aluminum tube of 41 mm outside diameter and 0.9 mm (nominal) wall thickness. Specimen tubes of different lengths were used in these tests; the details are given below. Piezoelectric (PCB) pressure gages along the detonation tube and test specimen were used to measure the detonation wave speed and pressure histories. Measurements of strain were also obtained and are discussed in the companion report by Shepherd et al. (2008).

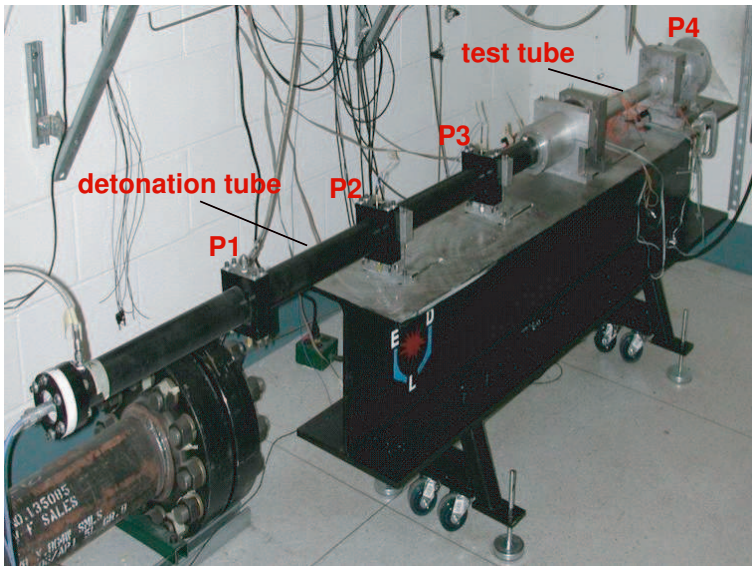

Figure 1: Detonation tube and specimen mounted on precision holding fixture.

3 Tests in 2005

The dimensions of the test specimen tube for shots 30-34 in 2005 are shown in Fig. 2. One pressure transducer was mounted in the middle of the test section and one was located at the end. The locations of the pressure transducers relative to the ignition point are shown in Table 1. The arrival times and the maximum pressures recorded at each transducer are listed in Table 2. The detonation waves propagated within -0.5% to +1% (see Fig. 3a) of the computed Chapman-Jouguet (CJ) velocity for these five tests. A comparison of the distance-time relationship for these tests is shown in Fig. 3b. The data are very repeatable with a small offset in arrival times for each data set. This offset is due to the intrinsic variability in the process of deflagration-to-detonation transition that is used to initiate the detonation. An average detonation velocity of 2357 ±12 m/s is computed by finding the average of slope to least squares fits of lines to the data in Fig. 3b.

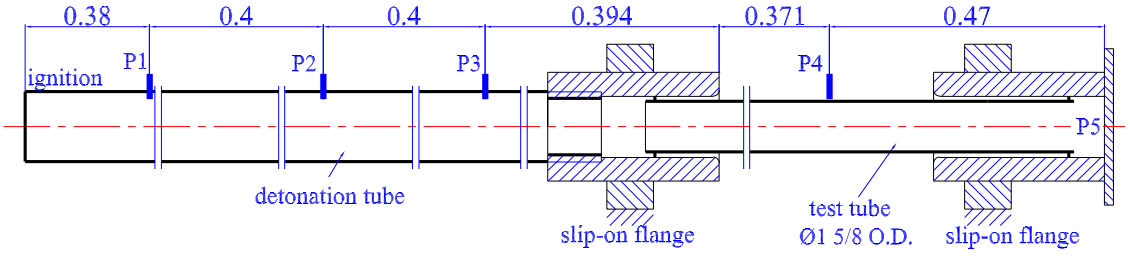

Figure 2: Tube dimensions for the shot 30-34 performed in 2005.

Figure 4 demonstrates the repeatability of the pressure signals from test to test. These results are all from gage P4 and the zero time of each signal has been shifted slightly to align the arrival time of the detonation for all five shots. We see that the fine details of the signal, which on first glance appear to be noise, are actually quite repeatable. These waves have a

Table 1: Location of pressure gauges.

Station	X (in)	X (m)
P_1	15	0.38
P_2	30.75	0.78
P_3	46.5	1.18
P_4	76.6	1.945
P_5	96	2.439

Table 2: Peak pressures and pressure wave arrival times for tests 30-34. The initial pressure is nominally 100 kPa for all tests.

shot	T_0 (K)	t_1 (ms)	P_1 (MPa)	t_2 (ms)	P_2 (MPa)	t_3 (ms)	P_3 (MPa)	t_4 (ms)	P_4 (MPa)	t_5 (ms)	P_5 (MPa)
30	296	0.389	5.22	0.556	4.28	0.723	4.43	1.62	3.22	1.25	8.162
31	297.5	0.397	5.27	0.568	4.13	0.734	4.52	1.05	3.30	1.26	7.79
32	297.3	0.426	5.31	0.600	4.03	0.764	4.47	1.08	3.12	1.31	9.07
33	296	0.366	4.33	0.538	4.02	0.709	4.50	1.03	3.42	1.25	10.13
34	296	0.421	4.37	0.593	3.95	0.764	4.42	1.08	3.19	1.27	8.103

period of approximately 2.5 μs or a frequency of 400 kHz. In order to make sure that the frequency content was being resolved, shot 34 was carried out with two digitizer channels connected to P4, one with a 2 MHz sampling rate and the other with a 4 MHz sampling rate; these are compared in Figs. 4b, c. Averaging all five signals together (thick black line in plots of Fig. 4), we see that aligning the pressure signal time of arrival preserves the 400 kHz oscillations and that the fine structure of the pressure history is not random but repeatable.

What is the origin of the high-frequency content in pressure signals of Fig. 4? Here are some possibilities:

1. Resonant response of the quartz elements in the piezo-electric pressure transducers. These gages (Piezotronics type 113A23) have a resonant frequency of >500 kHz according the company-provided information. The gages are also rated to measure shock rise times of less than 1 μs. Previous use of these gages in shock tube experiments in our laboratory with very well-defined wave forms do not show these oscillations.

2. Transverse shock waves associated with the detonation instability on the main front. The transverse wave spacing in these mixtures (Kaneshige and Shepherd, 1997) is on the order of 0.5 to 1.0 mm so that the the time separating the impingement of the waves on the transducers will be approximately 0.4-0.8 μs since the burned gas sound speed (App. C) is approximately 1.2 mm/μs. This corresponds to a frequency of 1.2 to 2.5 MHz, substantially higher than what is observed. The spacing of the transverse waves is also substantially smaller the active area of the transducer, 5.5 mm diameter, and the effect of the transverse waves will be averaged out over the face of the sensor. If the oscillations were due to transverse waves alone, we would expect the phasing of

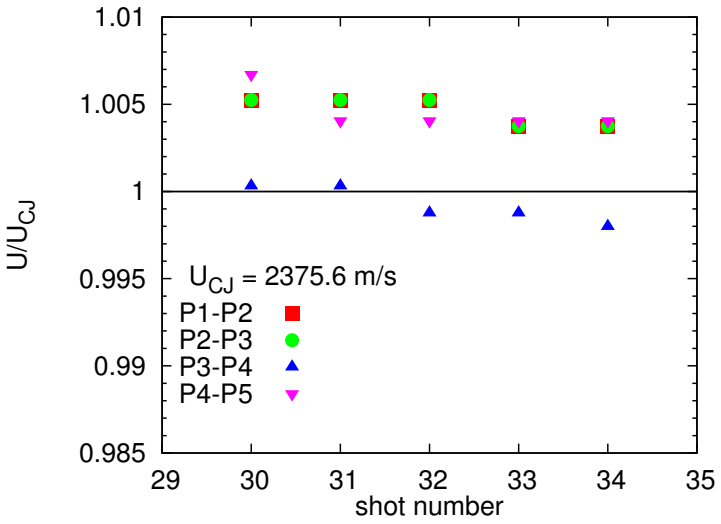

a)

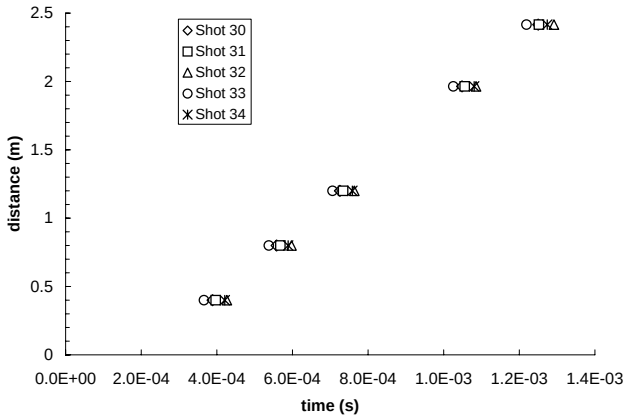

b)

Figure 3: a) Detonation velocity computed from the arrival times using pressure data of tests 30-34. b) Corresponding space-time diagram.

the transverse waves to be random and the features to average out

3. Shock waves that are relics of the initiation process. The initiation process proceeds by DDT through a Shchelkin spiral and very substantial transverse shock waves are known to be created by this process. The width of the coils (3 mm) and spacing of the spring (10 mm) used to construct the spiral is sufficiently smaller than the tube diameter that a much higher frequency content, on the order of 230-700 kHz, may be generated as the detonation passes through the final section of the spiral

4. Vibration of tubes coupling into the piezoelectric elements due to non-compensated accelerations. The tube vibrational frequencies were measured in related experiments and are on the order of 40 kHz, an order of magnitude lower than the observed frequency content. The signals are also observed prior to the main shock wave arrival (see P1, P2, P3 signals in the raw data plots in App. A) when this occurs and that is not the

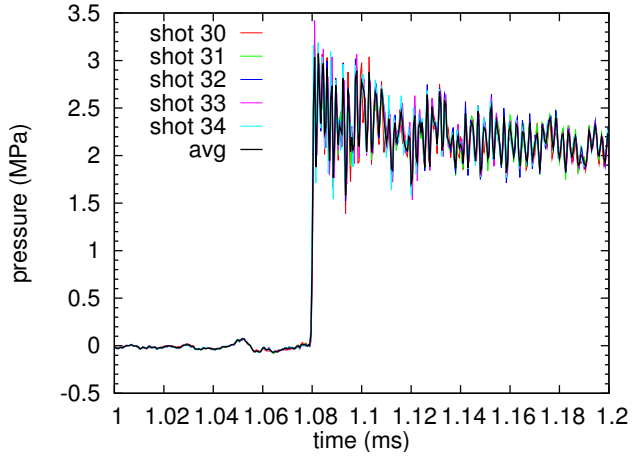

a)

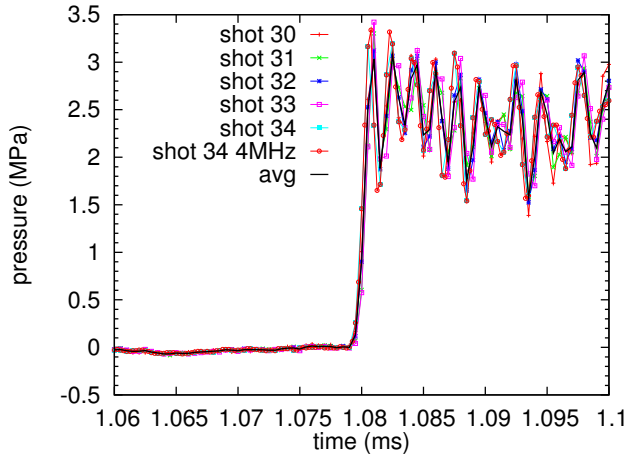

b)

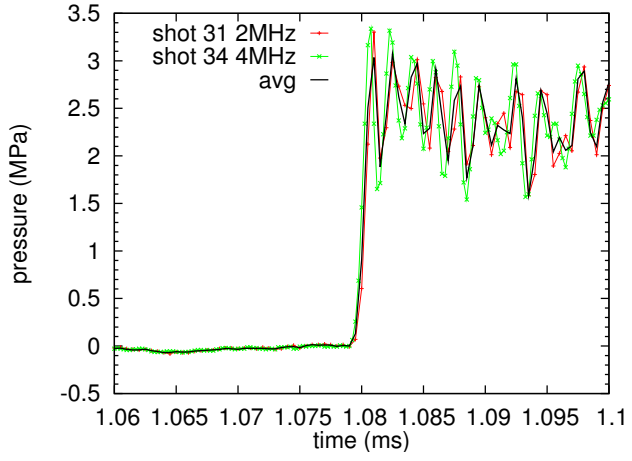

c)

Figure 4: Superimposed pressure traces for shots 30-34.

case for the P4 signals due to the difference in critical wave speed and gage mounting technique for P4 and P1-P3.

After considering these possibilities, we conclude that these features are physical in origin and associated with shock waves due to the initiation process. This conclusion is supported by a large number of observations in our laboratory on detonation wave propagation which show very similar features.

Following the initial set of experiments, comparisons of simulated and measured pressure traces at the various locations were carried out. Although the incident data were very repeatable and consistent with the CJ values, the measured peak pressures and arrival time for the reflected wave were not in as good agreement with the simulations. After careful analysis of the data, we found four main reasons for these discrepancies.

1. The distance between the ignition and the reflecting end was not properly measured.

2. The detonation speed computed based on the incident wave arrival time was slightly decreasing as the detonation propagated through the tube. This velocity variation was not considered in the simulations.

3. The five pressure transducers used in these tests had never been recalibrated since they were purchased.

4. Some pressure transducers were not thermally protected, and the pressure signals contained artifacts.

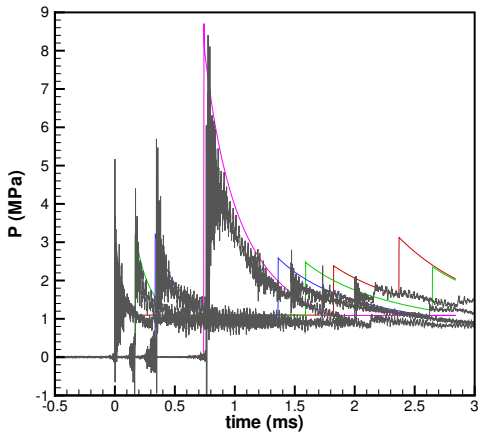

Figure 5: Comparison of computations and shot 31 at four stations after addressing problems 1, 2 and 3.

4 Tests in 2006

4.1 Modifications

To address the deficiencies in the 2005 tests, we made a number of changes (described below) and carried out new tests.

(1) Recalibration of pressure transducers

The pressure transducers were returned to the factory for evaluation and calibration. Table 3 lists the new conversion factors for the recalibrated pressure transducers.

Table 3: Conversion factors of the re-calibrated pressure transducers.

Station	Type	Conversion factor
P_1	113A24 SN 14835	702.5 mV/MPa
P_2	113A24 SN 13277	700.4 mV/MPa
P_3	113A24 SN 14771	732.4 mV/MPa
P_4	113A24 SN 13909	727.7 mV/MPa

After the first three problems were addressed, the comparison shown Fig. 5 was obtained.

(2) Modification of the reflecting ends.

In order to measure the strain signals close to the reflecting end, the previous slip-on flange was replaced with two plugs, one fits into the test tube end, and the other one mates with the collet, see App. D, Fig 35.

(3) Modification of clamps for mounting the pressure transducers

The critical wave speed (Beltman and Shepherd, 2002) for the detonation initiation tube (Fig 6) is about 2200 m/s, which is within 8% of the CJ detonation speed (2373.6 m/s) for C_2H_4+$3O_2$ mixtures at an initial pressure of 100 kPa and temperature of 23°C. As discussed in Beltman and Shepherd (2002), this will result in a resonant response of the tube wall that can produce artifacts in the pressure signals due to acceleration sensitivity of the piezoelectric pressure gauges. This is manifested as high-frequency oscillations observed ahead of the detonation front and superposed on the detonation wave pressure in the pressure traces of Fig. 5. To decrease the magnitude of the accelerations, we locally increased the tube stiffness with two new clamp assemblies (see App. D, Fig. 34) to hold the transducers to the tube. Pressure transducers were mounted on the top half of the clamp and the bottom half was mounted to the stiff work table. The improvement for the pressure signals was not as good as we expected, so we made further changes, discussed below.

(4) Improvement of reflecting pressure transducer signal

We added a piece of rubber between the test tube and the end cap to dampen the effect of tube oscillation on the pressure transducer mounted in the end cap.

Table 4: Notes for shots 1-7.

shot	P_0 (bar)	T_0 (K)	Mixture	Notes
1	0.4	295	$0.3H_2$+$0.7N_2O$	changes 1-2
2	0.4	296	$0.3H_2$+$0.7N_2O$	changes 1-2
3	0.4	296	$0.3H_2$+$0.7N_2O$	changes 1-2
4	0.99	297	C_2H_4+$3O_2$	changes 1-3
5	1.0	295	C_2H_4+$3O_2$	changes 1-4
6	0.9974	296	C_2H_4+$3O_2$	changes 1-2, 4-5
7	0.9995	297	C_2H_4+$3O_2$	changes 1-2, 4-5

(5) Modification of mounting pressure transducers

In the previous tests, pressure transducers were directly mounted on the tube and the seals were copper rings. We added a Swagelok adaptor between the tube and the pressure transducer. The rubber o-ring seal between the tube and the adaptor dampened the tube oscillation significantly.

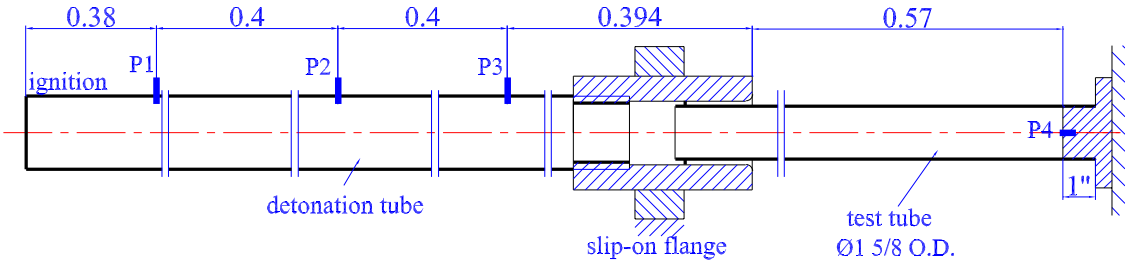

Figure 6: Tube dimensions for shots 1-7 performed in 2006.

4.2 Results

A total of 7 shots ware carried out with the modified setup, see Table 4 and 5 and Figs 23- 32. Shots 1-3 were performed only for validation of the initial tube setup. Shots 4-7 were used for comparison with the computations. Signals in shots 6 and 7 have the best quality of all the shots that were performed. The locations of the pressure transducers for these tests are listed in Table 6.

4.2.1 Experimental Uncertainties

The detonation wave arrival time data shown in Fig. 7 indicates that there is some variability in the DDT process that results in some scatter of the wave arrival at the first transducer. Subtracting the arrival time at gauge 1 from all subsequent gauges for a given test enables use to better compare tests. On this basis, the data are extremely consistent from test-to-test and the results can be represented as the average over all four tests. This is shown in Fig. 7 as the points labeled average.

Table 5: Arrival time of the incident wave as determined by time of peak pressure for shots 4-7.

shot	t_1 (ms)	$P_{1,max}$ (MPa)	t_2 (ms)	$P_{2,max}$ (MPa)	t_3 (ms)	$P_{3,max}$ (MPa)	t_4 (ms)	$P_{4,max}$ (MPa)
4	0.425	3.26	0.603	4.22	0.781	3.78	1.20	8.88
5	0.455	4.41	0.634	5.77	0.802	4.85	1.24	9.02
6	0.396	5.02	0.566	6.44	0.738	5.86	1.16	10.60
7	0.361	4.96	0.531	5.46	0.701	6.00	1.130	9.82

Table 6: Location of gauges.

Station	X (in)	X (m)
P_1	15	0.38
P_2	30.75	0.78
P_3	46.5	1.18
P_4	84.5	2.146

Although the data appear to be adequately fit by the straight line shown in Fig. 7, careful analysis shows that the wave speed is slightly decreasing as the wave propagates from gauge 1 to 4. Using a parabolic curve fit, a velocity of 2286.0 m/s is obtained at gauge 1 and 2100.9 m/s at gauge 4. These correspond to a deficit, $(U - U_{CJ})/U_{CJ}$, of -3.7% gauge 1 and -11.5% at gauge 4. The estimated single-sample uncertainty of the computed velocity between stations 1–2, 2–3 is 28 m/s and between stations 3–4 is 11 m/s. Given these values of the uncertainty in the individual observations, we conclude that the decrease in velocity between stations 1 and 4 is a real effect which is consistent with the data shown in Fig. 3. The deceleration of the wave is also consistent with observations on deflagration-to-detonation transition Ciccarelli and Dorofeev (2008) that show the detonation wave is overdriven, $U > U_{CJ}$, upon emerging from the transition event. The variation in wave velocity with distance is not accounted for in the simulations but instead an average value is used. A linear least-squares fit to the time-shifted data for shots 4–7 yields an average velocity of 2284 m/s with a standard deviation of 12 m/s. Compare this with the value obtained in 2005 (Section 3 of 2357 ±12 m/s. The systematic difference of 73 m/s far exceeds the standard deviation computed for either set of data.

We have also considered the influence of the uncertainty in the initial conditions using computations of the CJ wave speed for a range of initial compositions, pressures, and temperatures that correspond to the estimated range that results from the uncertainty in the facility operation and instrumentation. The composition is set using the method of partial pressures with an electronic capacitance pressure gauge (MKS Baratron Model 121A) with a full scale range of 1000 Torr and an accuracy of 0.5% of the reading and minimum resolution of 0.5 Torr. From these values we estimate the ethylene mole fraction to be 0.25 ±0.002. The average initial temperature was 23°C with a typical variation of 1°C and an additional instrument uncertainty of 1°C, so that the initial temperature range is 23 ± 2°C. The estimated range in initial pressure is 100 ± 0.5 kPa. The effect of individual variations

of each of these parameters on the computed (Browne et al., 2004) CJ velocity and pressure is shown in Table 7. A sample output from the program is given in Appendix C. From this sensitivity study, we observe that the potential variation in composition will contribute the most to uncertainty in the detonation velocity, U_{CJ} = 2373.6 ± 5 m/s. The effect of initial temperature and initial pressure variations on the computed CJ velocity are an order of magnitude smaller than the composition effects.

Table 7: Computed variation of CJ velocity and pressure as a function of the initial parameters.

P_0 (kPa)	T_0 (K)	$X_{ethylene}$	U_{CJ} (m/s)	P_{CJ} (MPa)
100.0	296.1	0.250	2373.6	3.361
100.0	296.1	0.252	2368.3	3.347
100.0	296.1	0.248	2378.9	3.374
100.5	296.1	0.250	2373.8	3.378
99.5	296.1	0.250	2373.3	3.343
100.0	298.1	0.250	2373.2	3.337
100.0	294.1	0.250	2374.0	3.384

Based on these uncertainty estimates, it appears that there is a systematic difference in the velocities between the two sets of data in 2005 and 2006 that cannot be explained by variations in composition or initial conditions. Other potential significant sources of uncertainty are the gage locations and arrival time measurements. Consider computing velocity from two gages located a distance X apart with the wave arrival time difference of T. From the arrival time velocity computation, we can compute the velocity uncertainty as

$$\frac{\delta U}{U} = \frac{\delta X}{X} - \frac{\delta T}{T} \tag{1}$$

where δX is the uncertainty in the gage position difference and δT is the uncertainty in the pressure arrival time difference.

Consider a typical gage spacing of X = 500 mm and a nominal wave speed of approximately 2300 m/s, which gives a nominal arrival time difference T = 215 μs. If the arrival times were measured precisely, then the observed wave speed difference $\delta U/U$ = -0.03 between 2005 and 2006 corresponds to a gage spacing difference of δX = -15 mm. If the gage spacing was measured precisely, then the observed wave speed difference corresponds to an arrival time difference of +6.45 μs. Based on the measurement capabilities in the lab, the gage spacing should have been known to ±1 mm and for a sampling speed of 2 MHz, the wave arrival time should be determined within ±1 μs.[1] This means that the measurement uncertainty should be at most ±5 m/s due to spatial location uncertainty and ± 12 m/s due to arrival time uncertainty. The observed difference is a factor of 4 times larger than

[1]The main source of uncertainty in this measurement is the selection of which peak to assign as the arrival time when the signals are noisy. This is most important for the gage on the reflecting end.

the maximum possible combined uncertainty which indicates a systematic error occurred in one of these sets of experiments. Based on post-test visual inspection and the location of witness marks made by the collets on the specimen tubes, we concluded that the error was in the position measurements for the 2005 tests.

4.3 Simulation Method

The simulations were carried out using AMROC Deiterding et al. (2006b) with a rigid confining tube. The detonation was simulated using a CV-burn model (see Deiterding et al. (2006a)) which gives product pressure profiles and detonation wave speeds that are very similar to the computationally more complex one-step model of reaction described by Deiterding et al. (2007). The CV-burn model has been extensively used in high-explosive simulations as discussed by Bdzil et al. (2001) and although the details of the reaction process are not resolved, this technique is computationally efficient for a problem where the dynamics of the detonation products are of interest. This is the case in the present problem.

The flow is simulated using the one-dimensional Euler model of a perfect gas with energy addition. The specific energy release used to simulate the detonation was $q = 4{,}704{,}080$ J/kg and the ratio of specific heats was constant $\gamma = 1.24$. The computed CJ detonation velocity using these parameters is 2291.7 m/s, which is selected to approximate the observed average velocity of 2285 m/s shown in Fig. 7. The parameters are not completely consistent with the thermodynamics of the products but give the best results for the comparison of the data and simulation. As discussed by Radulescu and Hanson (2005) and Wintenberger et al. (2004) and also used in previous computations (Shepherd et al., 1991) of wave motion in detonation products, the appropriate values of the specific heat ratio is closer to the equilibrium value of 1.14 rather than the post-shock frozen value of 1.24.

4.4 Comparison

Data from Shots 4 and 7 are compared with simulation results in Fig 8 and Fig 9. The measured arrival times of the incident waves at four stations, as well as the pressure history, now show excellent agreement with simulations for incident waves. The experiment peak pressures are substantially higher than the simulated values but this is typical of unfiltered experimental data which shows large amplitude pressure fluctuations superposed on the general trend of a shock followed by an expansion wave. The high frequency signals are not noise but a combination of secondary shock waves (transverse waves and transients from the initiation) and artifacts due to the acceleration sensitivity of the gauges and vibration of the tube wall. The experimentally measured pressure behind the reflected wave is systematically lower than the simulated values. The agreement between experiment and simulation is now reasonable for the reflected waves but there remain systematic differences between simulations and data for the arrival time and amplitudes.

There are several possible explanations for the remaining systematic differences between simulation and experiment that we have considered:

1. The fluid dynamics model is highly idealized and does not account for heat loss to the tube walls. Radulescu and Hanson (2005) show that this effect is significant in tubes

of this length and can result in up to a 10% difference in the thermodynamic state of the products that the reflected waves are propagating through.

2. The thermodynamic model of the detonation products does not account for the correct relationship between enthalpy (or internal energy) and temperature. A two-gamma or detailed model of the thermochemistry would be needed to resolve this.

3. The simulation does account for the turbulent motion and nonuniform state that must exist sufficiently far behind the detonation front. The turbulent flow will be associated with a spatially nonuniform thermodynamic state and will cause more rapid attenuation of the reflected shock waves than predicted by the idealized simulation.

4. There are heat transfer and gauge response effects on the measured peak pressures. Heat transfer becomes increasingly important at longer time scales.

5. The pressure transducer signals still show significant contamination due to acceleration sensitivity and vibration in the tube walls.

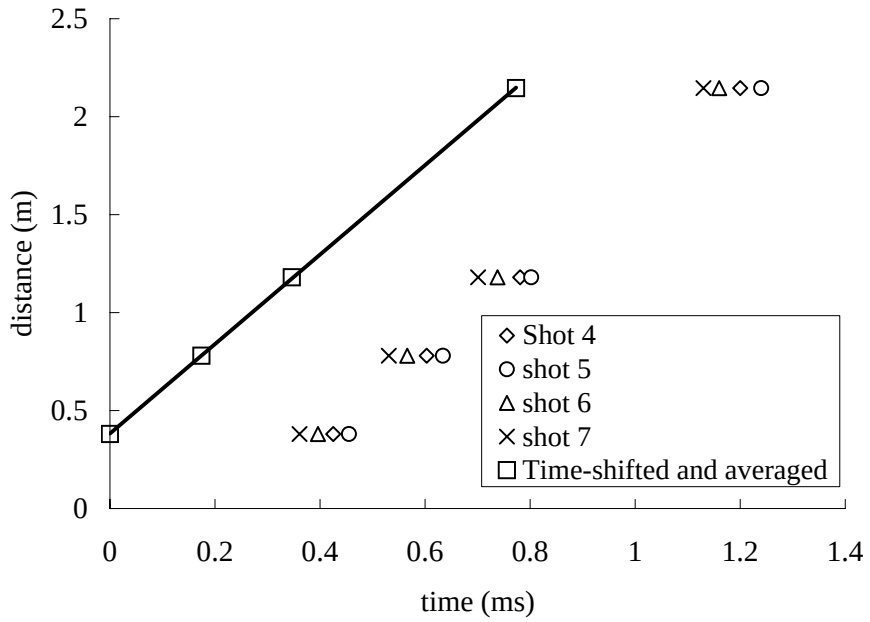

Figure 7: Arrival time of the incident wave (peak pressure time) vs. location of the pressure gauges. $X = 0$ is the ignition location. Prior to averaging, the time values were shifted by subtracting the arrival time at gauge 1 for each shot. The trend line is a linear least-squares fit to the average values of arrival time.

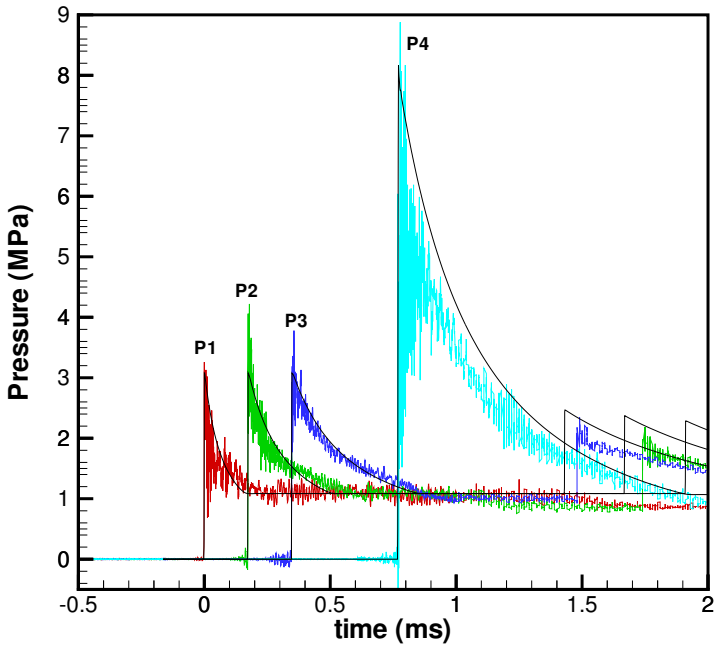

Figure 8: Comparison of simulations and shot 4 at four locations.

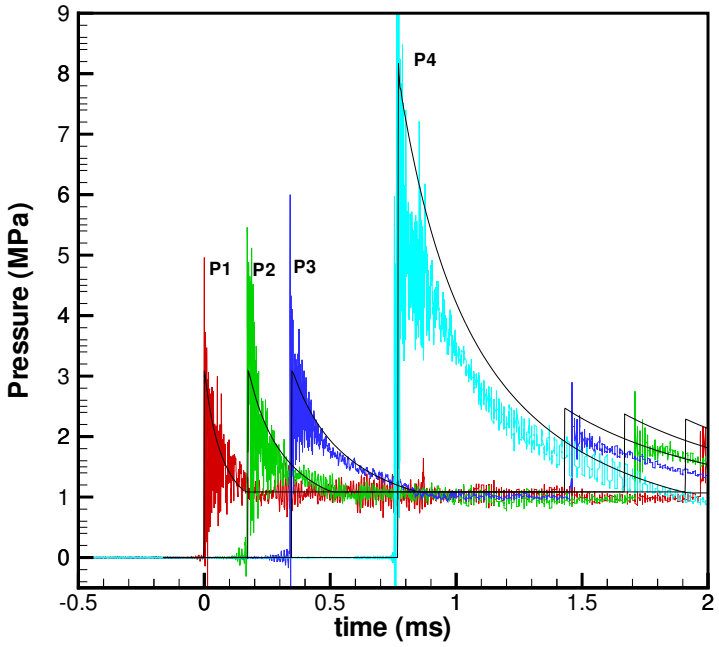

Figure 9: Comparison of computations and shot 7 at four locations.

5 Ideal Detonation Model

The Chapman-Jouguet (CJ) model of an ideal detonation (Fickett and Davis, 1979) can be combined with the Taylor-Zeldovich (TZ) similarity solution (Zel'dovich and Kompaneets, 1960, Taylor, 1950) to obtain an analytic solution to the flow field behind a steadily-propagating detonation in a tube.[2] The most common situation in laboratory experiments is that the detonation wave starts at the closed end of the tube and the gas in the tube is initially stationary, with flow velocity $u_1 = 0$. This solution can be constructed piecewise by considering the four regions shown on Figure 10; the stationary reactants ahead of the detonation mixture (state 1); the detonation wave between states 1 and 2; the expansion wave behind the detonation (between states 2 and 3); and the stationary products next to the closed end of the tube, state 3.

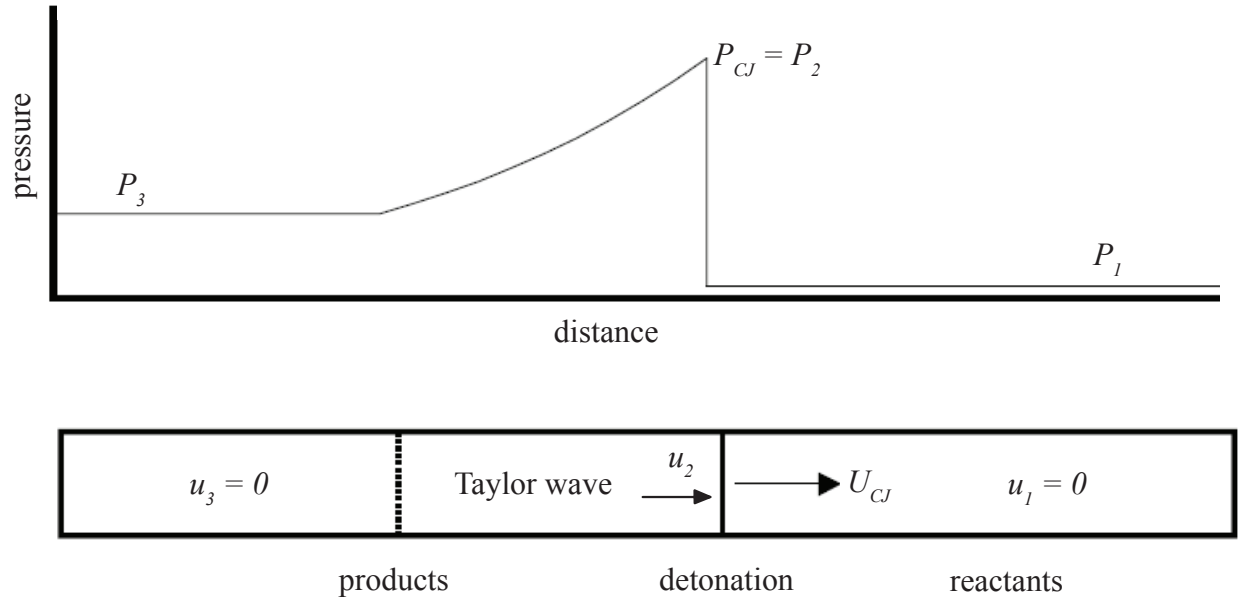

Figure 10: Detonation propagation in tube with a closed end.

In this model, the detonation travels down the tube at a constant speed U, equal to the Chapman-Jouguet velocity U_{CJ}. The corresponding peak pressure, P_2, is the Chapman-Jouguet pressure P_{CJ}. The structure of the reaction zone and the associated property variations such as the Von Neumann pressure spike are neglected in this model. The detonation wave instantaneously accelerates the flow and sets it into motion $u_2 > 0$, then the expansion wave gradually brings the flow back to rest, $u_3 = 0$. As an ideal detonation wave propagates through the tube, the expansion wave increases in width proportionally so that the flow always appears as shown in Fig. 10 with just a change in the scale of the coordinates. This is true only if we neglect non-ideal processes like friction and heat transfer within the expansion wave. If the tube is sufficiently slender (length/diameter ratio sufficiently large),

[2]This section is condensed from Browne et al. (2004). See that report for a more in-depth discussion and more references.

friction and heat transfer will limit the growth of the expansion wave.

6 Detonation Wave Relationships

The equations of mass, momentum and energy conservation across the wave (Thompson, 1972) are most conveniently solved in a coordinate system that moves with the detonation wave speed U. The velocity components are

$$w_1 = U - u_1 \tag{2}$$

and

$$w_2 = U - u_2 \ . \tag{3}$$

The jump conditions are simply the conservation of mass, momentum and energy in this frame:

$$\begin{aligned} \rho_1 w_1 &= \rho_2 w_2 \ , & (4)\\ P_1 + \rho_1 w_1^2 &= P_2 + \rho_2 w_2^2 \ , & (5)\\ h_1 + \frac{w_1^2}{2} &= h_2 + \frac{w_2^2}{2} \ , & (6)\\ s_2 &\geq s_1 \ . & (7) \end{aligned}$$

The mass and momentum conservation equations can be combined to obtain a relationship between pressure and velocity as a function of wave speed known as the *Rayleigh line*

$$P_2 - P_1 = -\left(\rho_1 w_1\right)^2 \left(v_2 - v_1\right) \tag{8}$$

and this result can be combined with mass and energy conservation equations to obtain the *Hugoniot curve*

$$h_2 - h_1 = \frac{1}{2}\left(P_2 - P_1\right)\left(v_2 + v_1\right) \ . \tag{9}$$

Instead of the wave or flow velocities, the Mach number

$$M = w/a \tag{10}$$

is more convenient for analytical formulas. The sound speed a is defined as

$$a = \sqrt{\frac{\partial P}{\partial \rho}\bigg)_s} \ . \tag{11}$$

The solution to the jump conditions can be graphically represented (Fig. 11) in the pressure-velocity plane as the intersection of the Hugoniot curve (9) and Rayleigh lines (8). As shown, there are no solutions for wave speeds $U < U_{CJ}$, one solution possible for $U = U_{CJ}$, and two for $U > U_{CJ}$. From this geometrical construction, the minimum wave speed corresponds to a point of tangency between the Hugoniot curve and Rayleigh line.

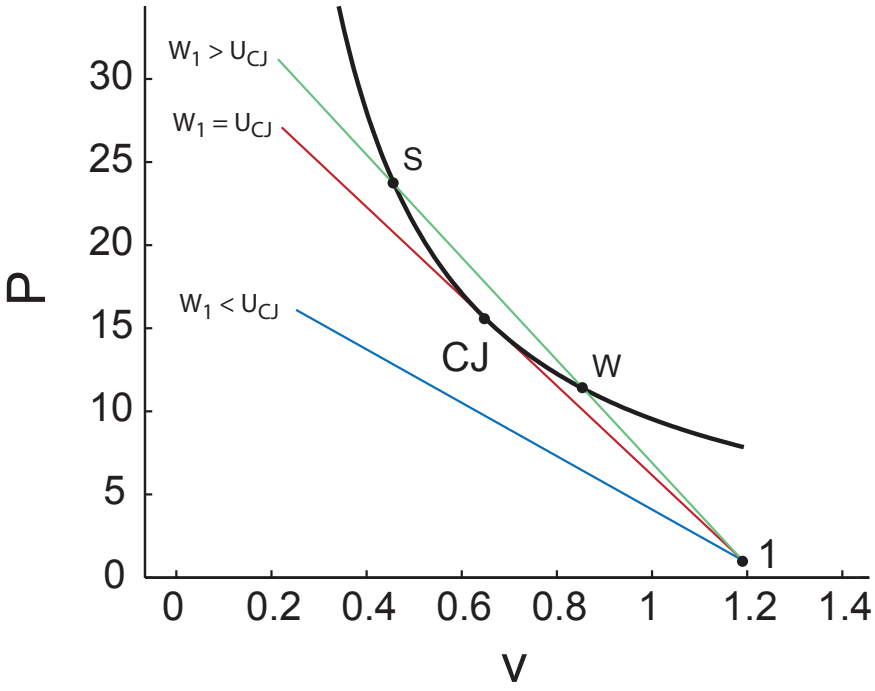

Figure 11: Hugoniot curve and three representative Rayleigh lines illustrating the minimum wave speed character of the CJ solution.

6.1 Chapman-Jouguet Conditions

For a detonation, the flow upstream of the wave is supersonic $M_1 > 1$ and the flow downstream is either subsonic or sonic, $M_2 \leq 1$.[3] Ideal detonation waves are assumed to propagate at the minimum possible speed that is consistent with the conservation relationships for a steady wave (Fickett and Davis, 1979). This minimum detonation wave speed is the Chapman-Jouguet (CJ) velocity, $U_{min} = U_{CJ}$ shown on Fig. 11. At the minimum speed, Hugoniot and Rayleigh lines are tangent at the CJ point

$$\frac{P_{CJ} - P_1}{v_{CJ} - v_1} = \frac{\partial P}{\partial v}\Big)_{Hugoniot} = -\frac{w_2^2}{v_2^2} \,. \tag{12}$$

By combining the Hugoniot curves with the fundamental relationship of thermodynamics, the entropy can be shown Fickett and Davis (1979), Thompson (1972) to be a minimum at the detonation CJ point. This means that the Hugoniot and isentrope are also tangent at the CJ point

$$\frac{\partial P}{\partial v}\Big)_{Hugoniot} = \frac{\partial P}{\partial v}\Big)_{s} = -\frac{a_2^2}{v_2^2} \,. \tag{13}$$

[3]For sufficiently fast waves, $U > U_{CJ}$, it is theoretically possible to find two solutions for the downstream state, one is subsonic $M_2 < 1$ (state "S" on Fig. 11) and one is supersonic $M_2 > 1$ (state "W" on Fig. 11). Only in exception cases can the supersonic solution be obtained and we will restrict our considerations to the conventional solution with $M_2 \leq 1$.

Combining these two expressions, we find that the product velocity is *sonic relative to the wave* at the CJ point is

$$w_{2,CJ} = a_2 \ , \tag{14}$$

or

$$M_2 = 1 \quad \text{when} \quad M_1 = M_{CJ} \ . \tag{15}$$

This version of the CJ condition is used subsequently in the analytic solution of the jump conditions to obtain an explicit expression for the CJ speed.

6.2 Ideal gas model

The properties downstream of the wave can be determined analytically (Thompson, 1972) by using an ideal gas equation of state and assuming constant heat capacity to solve the jump conditions that treat the detonation as a discontinuity. A widely used version of this model uses different properties in the reactants and products (pp. 347-359 of Thompson, 1972) and assumes a value of the energy release q, different values of γ and R in reactants and products. These parameters can be determined by equilibrium computations based on realistic thermochemical properties and a mixture of the relevant gas species in reactants and products. Examples of the results of these computations are given in Shepherd and Schultz. The model equations are:

$$h_1 = c_{p1} T \ , \tag{16}$$
$$h_2 = c_{p2} T - q \ , \tag{17}$$
$$P_1 = \rho_1 R_1 T_1 \ , \tag{18}$$
$$P_2 = \rho_2 R_2 T_2 \tag{19}$$

where

$$c_{p1} = \frac{\gamma_1 R_1}{\gamma_1 - 1} \ , \tag{20}$$
$$c_{p2} = \frac{\gamma_2 R_2}{\gamma_2 - 1} \ , \tag{21}$$
$$R_1 = \frac{\mathcal{R}}{W_1} \ , \tag{22}$$
$$R_2 = \frac{\mathcal{R}}{W_2} \ , \tag{23}$$
$$a_1 = \sqrt{\gamma_1 R_1 T_1} \ , \tag{24}$$
$$a_2 = \sqrt{\gamma_2 R_2 T_2} \ , \tag{25}$$
$$M_1 = w_1 / a_1 \ , \tag{26}$$
$$M_2 = w_2 / a_2 \ . \tag{27}$$

Substitute the ideal gas model into the jump conditions and after some algebra, we obtain the following relationships between properties upstream and downstream of the detonation wave:

$$\frac{P_2}{P_1} = \frac{1+\gamma_1 M_1^2}{1+\gamma_2 M_2^2}\,, \tag{28}$$

$$\frac{v_2}{v_1} = \frac{\gamma_2 M_2^2}{\gamma_1 M_1^2} \cdot \frac{1+\gamma_1 M_1^2}{1+\gamma_2 M_2^2}\,, \tag{29}$$

$$\frac{T_2}{T_1} = \frac{\gamma_1 R_1}{\gamma_2 R_2} \cdot \frac{\dfrac{1}{\gamma_1 - 1} + \dfrac{1}{2} M_1^2 + \dfrac{q}{a_1^2}}{\dfrac{1}{\gamma_2 - 1} + \dfrac{1}{2} M_2^2}\,. \tag{30}$$

6.3 Ideal-gas Two-γ CJ Model

Substituting the CJ condition (15) into the analytic solution for the detonation jump conditions yields an expression for the detonation[4] CJ velocity or Mach number

$$M_{CJ} = \sqrt{\mathcal{H} + \frac{(\gamma_1+\gamma_2)(\gamma_2-1)}{2\gamma_1(\gamma_1-1)}} + \sqrt{\mathcal{H} + \frac{(\gamma_2-\gamma_1)(\gamma_2+1)}{2\gamma_1(\gamma_1-1)}}\,, \tag{31}$$

where the parameter $\mathcal{H}$ is the nondimensional energy release

$$\mathcal{H} = \frac{(\gamma_2-1)(\gamma_2+1)q}{2\gamma_1 R_1 T_1}\,. \tag{32}$$

The other properties can be found by substitution into the general solutions given above

$$\frac{P_{CJ}}{P_1} = \frac{\gamma_1 M_{CJ}^2 + 1}{\gamma_2 + 1}\,, \tag{33}$$

$$\frac{\rho_{CJ}}{\rho_1} = \frac{(\gamma_2+1)}{\gamma_2} \cdot \frac{1}{(1 + \dfrac{1}{\gamma_1 M_{CJ}^2})}\,, \tag{34}$$

$$\frac{T_{CJ}}{T_1} = \frac{P_{CJ}}{P_1} \cdot \frac{R_1 \rho_1}{R_2 \rho_{CJ}}\,, \tag{35}$$

$$u_{CJ} = U\left(1 - \frac{\rho_1}{\rho_2}\right)\,. \tag{36}$$

7 Relationship of Ideal Model parameters to Real Gas Properties

The two-γ model contains six parameters (R_1, γ_1, R_2, γ_2, q, U_{CJ} or M_{CJ}) that have to be determined from computations with a realistic thermochemical model and chemical equilibrium in the combustion products. This can be done with the programs provided in the

[4]There are two solutions to the equations, one is the detonation solution $M_1 > 1$, the other is the deflagration solution $M_1 < 1$. The deflagration solution is a limiting case of a subsonic flame and is not relevant to ideal detonations.

Shock and Detonation Toolbox which uses the Cantera software for carrying out the thermochemical and equilibrium computations. The theory and use of the programs is described by Browne et al. (2004).

The parameters are:

$$R_1 = \frac{\mathcal{R}}{W_1} \, , \tag{37}$$

where the universal gas constant (SI units) is

$$\mathcal{R} = 8314. \, \mathrm{J} \cdot \mathrm{kmol}^{-1} \cdot \mathrm{K}^{-1} \, . \tag{38}$$

The mean molar mass is computed from the composition of the gas and the mixture formula

$$W = \sum_{i-1}^{K} X_i W_i \tag{39}$$

where X_i is the mole fraction of species i and W_i is the molar mass of species i. The value of γ for the reactants can be interpreted as the ratio of the specific heats

$$\gamma_1 = \frac{C_{p,1}}{C_{v,1}} \, . \tag{40}$$

This is identical to the logarithmic slope of the *frozen* isentrope

$$\gamma_{fr} = -\frac{v}{P} \frac{\partial P}{\partial v}\Big)_{s,fr} = \frac{a_{fr}^2}{Pv} \, , \tag{41}$$

where the subscript *fr* indicates that the composition is held fixed or frozen. In order to compute the downstream state 2, we need to first find the CJ velocity which requires using software like the minimum velocity CJ algorithm implemented in Python or Matlab in the Shock and Detonation Toolbox.

Once the CJ conditions have been computed, the CJ state must be evaluated. This can be done using the jump condition solution algorithm implemented in Python or Matlab in the Shock and Detonation Toolbox. The CJ state includes the mean molar mass W_2 and the value of the parameter γ_2 can be obtained from the logarithmic slope of the *equilibrium* isentrope

$$\gamma_{eq} = -\frac{v}{P} \frac{\partial P}{\partial v}\Big)_{s,eq} \, , \tag{42}$$

where the subscript eq implies that the derivative is carried out with shifting composition to maintain equilibrium. The value of the equilibrium sound speed can be used to find the numerical value of γ_{eq}

$$\gamma_{eq} = \frac{a_{eq}^2}{Pv} \, . \tag{43}$$

Once these parameters have been defined, the value of the parameter q can be obtained by solving the two-γ relationships (34), (35), and (36) to eliminate pressure, volume and temperature

$$q = a_1^2 \left[\frac{(1+\gamma_1 M_1^2)^2}{2(\gamma_2^2 - 1)} \left(\frac{\gamma_2}{\gamma_1} \right)^2 \frac{1}{M_1^2} - \frac{1}{\gamma_1 - 1} - \frac{M_1^2}{2} \right] . \tag{44}$$

If the one-γ model is used, then this expression simplifies to

$$q = \frac{a_1^2}{2(\gamma^2 - 1)} \left(M_{CJ} - \frac{1}{M_{CJ}} \right)^2 . \tag{45}$$

7.1 Example: Ethylene-Oxygen Detonation

A stoichiometric mixture of ethylene and oxygen has the composition

$$C_2H_4 + 3O_2$$

so that $X_{C2H4} = 0.25$ and $X_{O2} = 0.75$. The results of using the Cantera program CJstate_isentrope to compute the CJ velocity and state for initial conditions of 295 K and 1 bar are:

```
Initial pressure 100000 (Pa)
Initial temperature 295 (K)
Initial density 1.2645 (kg/m3)
a1 (frozen) 325.7368 (m/s)
gamma1 (frozen) 1.3417 (m/s)

Computing CJ state and isentrope for C2H4:1 O2:3.01 using gri30_highT.cti
CJ speed 2372.1595 (m/s)
CJ pressure 3369478.0035 (Pa)
CJ temperature 3932.4868 (K)
CJ density 2.3394 (kg/m3)
CJ entropy 11700.9779 (J/kg-K)
w2 (wave frame) 1282.1785 (m/s)
u2 (lab frame) 1089.9809 (m/s)
a2 (frozen) 1334.5233 (m/s)
a2 (equilibrium) 1280.6792 (m/s)
gamma2 (frozen) 1.2365 (m/s)
gamma2 (equilibrium) 1.1388 (m/s)
```

From the program output and gas objects computed by Cantera, we find the following parameters in Table 8

Table 8: Parameters for a CJ detonation in stoichiometric ethylene-oxygen computed by the Shock and Detonation Toolbox.

W_1	(kg/kmol)	31.0
a_1	(m/s)	325.7
γ_1		1.342
W_2	(kg/kmol)	23.45
a_2	(m/s)	1280.
γ_2		1.139
U_{cJ}	(m/s)	2372.
M_{CJ}		7.28
q	(MJ/kg)	9.519

8 Taylor-Zeldovich Expansion Wave

The properties within the expansion wave can be calculated by assuming a similarity solution (Zel'dovich and Kompaneets, 1960, Taylor, 1950) with all properties a function $f(x/Ut)$. For a planar flow, the simplest method of finding explicit solutions is with the method of characteristics . There are two[5] sets of characteristics, C^+ and C^- defined by

$$C^+ \qquad \frac{dx}{dt} = u + a \,, \tag{46}$$

$$C^- \qquad \frac{dx}{dt} = u - a \,. \tag{47}$$

On the characteristics the Riemann invariants $J^{\pm}$ are defined and are constants in the smooth portions of the flow. In an ideal gas, the invariants are (Thompson, 1972):

$$\text{on} \quad C^+ \qquad J^+ = u + F \,, \tag{48}$$

$$\text{on} \quad C^- \qquad J^- = u - F \,. \tag{49}$$

The Riemann function F is defined as

$$F = \int_{P_\circ}^{P} \frac{dP'}{\rho a} \,, \tag{50}$$

where $P_\circ$ is a reference pressure and the integral is computed along the isentrope $s_\circ$ passing through states 2 and 3. For an ideal gas, the integral can carried out and the indefinite integral is equal to

$$F = \frac{2a}{\gamma - 1} \,. \tag{51}$$

[5]There are actually three, but the third one corresponding to the flow speed u does not have to be considered if we assume the flow in the expansion wave is isentropic.

In this section, the value of γ is everywhere taken to be the equilibrium value in the detonation products.

The solution proceeds by recognizing that within the expansion fan, $a_3 \geq x/t \geq U_{CJ}$, the C^+ characteristics are simply rays emanating from the origin of the x-t coordinate system and between the end of the expansion fan and the wall, $0 \geq x/t \geq a_3$, the characteristics are straight lines (Thompson, 1972).

$$\begin{aligned} \frac{dx}{dt} = u + a = \frac{x}{t} \qquad &\text{for} \qquad a_3 < \frac{x}{t} < U_{CJ} \ , \\ \frac{dx}{dt} = a_3 \qquad &\text{for} \qquad 0 < \frac{x}{t} < a_3 \ . \end{aligned} \tag{52}$$

The characteristics C^- span the region between the detonation and the stationary gas and on these characteristics the Riemann invariant J^+ is constant. Evaluating J^- at states 2 and 3 yields the value of the sound speed in region 3 in terms of the properties of state 2, the CJ state,

$$J^- = u - \frac{2}{\gamma - 1} a = -\frac{2}{\gamma - 1} a_3 = u_2 - \frac{2}{\gamma - 1} a_2 \ . \tag{53}$$

From the CJ condition we have

$$u_2 = U_{CJ} - a_{CJ} \ , \tag{54}$$

and the sound speed in region 3 is

$$a_3 = \frac{\gamma + 1}{2} a_{CJ} - \frac{\gamma - 1}{2} U_{CJ} \ . \tag{55}$$

The variation of properties within the expansion wave can be determined using the similarity properties of the C^+ characteristics and the relationship between velocity and sound speed on the C^- characteristics:

$$\frac{a}{a_3} = 1 - \frac{\gamma - 1}{\gamma + 1} \left(1 - \frac{x}{a_3 t} \right) \ . \tag{56}$$

The other properties within the expansion fan can be found using the fact that the flow is isentropic in this region.

$$\frac{a}{a_3} = \left(\frac{T}{T_3} \right)^{\frac{1}{2}} \quad ; \quad \frac{P}{P_3} = \left(\frac{\rho}{\rho_3} \right)^{\gamma} \quad ; \quad \frac{T}{T_3} = \left(\frac{\rho}{\rho_3} \right)^{\gamma - 1} \tag{57}$$

where T is the temperature, ρ is the density and P is the pressure. The subscript 3 refers to the conditions at the end of the expansion wave. The pressure P_3 is calculated from

$$P_3 = P_{CJ} \left(\frac{a_3}{a_{CJ}} \right)^{\frac{2\gamma}{\gamma - 1}} \ . \tag{58}$$

This finally gives for the pressure in the expansion wave

$$P = P_3 \left(1 - \left(\frac{\gamma - 1}{\gamma + 1} \right) \left[1 - \frac{x}{c_3 t} \right] \right)^{\frac{2\gamma}{\gamma - 1}} \ . \tag{59}$$

8.1 Determining Realistic TZ parameters

The states on the product isentrope need to be determined numerically, starting at the CJ point and extending to state 3. This is carried out in the program CJstate_isentrope to numerically determine the value of thermodynamic properties such as density, sound speed, and temperature

$$\rho = \rho(P, s = s_{CJ}) \ , \tag{60}$$
$$a = a(P, s = s_{CJ}) \ , \tag{61}$$
$$T = T(P, s = s_{CJ}) \ , \tag{62}$$

and also velocity in the TZ wave,

$$u = u_2 + \int_{P_{CJ}}^{P} \frac{dP'}{(\rho a)_{s=s_{CJ}}} \ , \tag{63}$$

parametrically as a function of pressure. The state 3 can be found by numerically solving the integral equation

$$u_2 = \int_{P_{CJ}}^{P_3} \frac{dP}{(\rho a)_{s=s_{CJ}}} \tag{64}$$

obtained by equating the Riemann invariant on the characteristic connecting states 2 and 3. In the program, the integral is carried out by using the trapezoidal rule with on the order of 100-200 increments on the isentrope. Interpolation is used to find state 3.

For the stoichiometric mixture of ethylene and oxygen discussed previously, the computation of state 3 using the Shock and Detonation Toolbox gives the following values.

```
Generating points on isentrope and computing Taylor wave velocity
State 3 pressure 1225686.0898 (Pa)
State 3 temperature 3608.3006 (K)
State 3 volume 1.0434 (m3/kg)
State 3 sound speed (frozen) 1253.7408 (m/s)
State 3 sound speed (equilibrium) 1201.0748 (m/s)
State 3 gamma frozen) 1.2291 (m/s)
State 3 gamma (equilibrium) 1.128 (m/s)
```

We note that there is a small change in γ_2 with the change in pressure on the isentrope and the pressure at state 3 is approximately $0.36 P_{CJ}$.

9 Approximating the TZ Wave

The property variations within the ideal detonation wave are now completely specified. For example, the exact solution for the pressure profile is

$$P(x,t) = \begin{cases} P_1 & U_{CJ} < x/t < \infty \\ P_3 \left(1 - \left(\frac{\gamma-1}{\gamma+1}\right)\left[1 - \frac{x}{a_3 t}\right]\right)^{\frac{2\gamma}{\gamma-1}} & a_3 < x/t < U_{CJ} \\ P_3 & 0 < x/t < a_3 \end{cases} \ . \tag{65}$$

In analytical studies, it is useful to approximate the dependence of the pressure within the expansion wave with a simpler function. Experimenting with several functional forms shows that an exponential can be used to represent this variation. This was used by Beltman and Shepherd (2002) as a model of the loading function for elastic wave computations. At a fixed point in space, the variation of pressure with time can be represented by

$$P(x,t) = \begin{cases} P_1 & 0 < t < t_0 \\ (P_2 - P_3)\exp\left(-(t-t_o)/\tau\right) + P_3 & t_0 < t < \infty \end{cases} , \tag{66}$$

where t_0 is the time it takes for a detonation to travel from the origin to the measurement location x. For an ideal detonation wave $t_0 = x/U_{CJ}$, for non-ideal waves or matching with experimental data, t_0 can be specified to match experimental or computed arrival times. The time constant τ can be determined by fitting the exponential relationship to the exact expression. The exact expression for pressure in the expansion wave can be rewritten as

$$P(x,t) = P_3\left[1 + \frac{\gamma-1}{\gamma+1}\left(\frac{U_{CJ}/c_3 - 1 - t'/t_{CJ}}{1 + t'/t_{CJ}}\right)\right]^{\frac{2\gamma}{\gamma-1}} , \tag{67}$$

where $t' = t$ - t_{CJ}. This form of the TZ solution is particularly useful for comparison with experimental data if we equate $t' = t$ - t_0, where t_0 is the arrival time of the wave at the station of interest. The parameter U_{CJ}/c_3 does not have to be computed independently if P_{CJ}, P_3 and γ are known or can estimated. Setting $t' = 0$ in (67), we find that

$$\frac{U_{CJ}}{c_3} = \frac{\gamma+1}{\gamma-1}\left[\left(\frac{P_{CJ}}{P_3}\right)^{\frac{\gamma-1}{2\gamma}} - \frac{2}{\gamma+1}\right] . \tag{68}$$

By inspection of the argument in (67), we conclude that the time constant τ should have the form

$$\tau = t_{CJ} f(\gamma, U_{CJ}/c_3) , \tag{69}$$

where f is a nondimensional function of the variables γ and U_{CJ}/c_3. Computations of the two parameters using the one-γ model shows that $1.9 < a_3/U_{CJ} < 2$ for a wide range of values of γ and detonation Mach numbers $5 < M_{CJ} < 10$. Fitting the exponential function to the pressure variation in the expansion wave for this range of parameters yields $0.31 < \tau/t_{CJ} < 0.34$. A useful approximation is

$$\tau \approx \frac{t_{CJ}}{3} . \tag{70}$$

In actual practice, if we are trying to represent the variation of pressure over a limited portion of a detonation tube, it is sufficient to take τ to be a constant and this can be evaluated at some intermediate location within the portion of the tube that is of interest.

The analytic Taylor-Zeldovich wave and the approximate fit are compared to the averaged data for transducer station 4 shots 30-34 in Fig. 12. The time origin for the analytic and approximate solutions has been shifted to the experimental wave arrival time of 1.081 ms to enable direct comparison of the waveforms. The experimental data are shown only up to the time of arrival of the reflected shock wave. The computed CJ pressure (3.37 MPa),

detonation velocity (2372.2 m/s), plateau pressure (1.226 MPa), and equilibrium value of $\gamma = 1.1388$ were used to evaluate the exact solution. The CJ pressure was adjusted to 3.1 MPa, the plateau pressure kept as 1.226 MPa, and the time scale of 0.276 ms was used in the approximate solution. The slight decrease (8%) in peak pressure yields better agreement between the approximate solution and the data. The time constant choice of $\tau = t_{cj}/3$ appears to be reasonable.

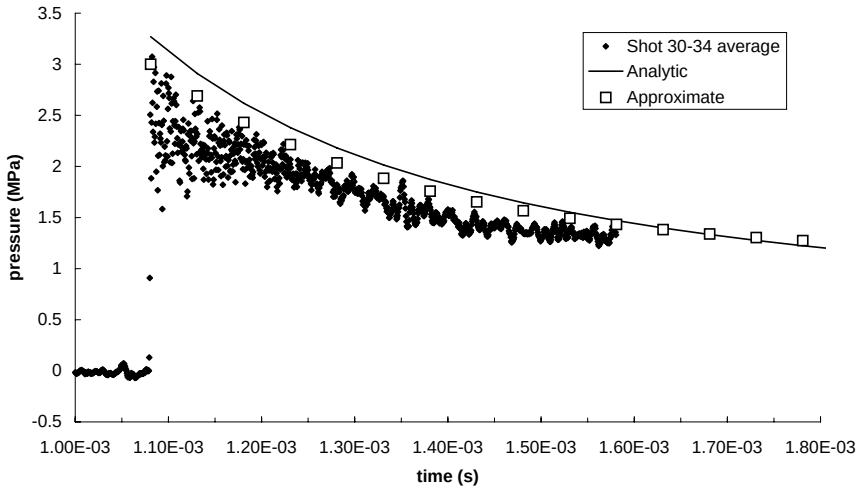

Figure 12: Comparison of average pressure signals from location 4 (1.964 m) in shots 30-34 with exact Taylor-Zeldovich solution and approximate fit.

10 Comparison of Two-Gamma and Real gas models

For the stoichiometric ethylene-oxygen example discussed in the text, the two-γ and real gas results are compared in detail in Table 9.

Table 9: Comparison of real gas and two-γ results for a CJ detonation in stoichiometric ethylene-oxygen.

Parameter	SD Toolbox Value	2-γ Model
M_{CJ}	7.282	7.287
P_2/P_1	33.69	33.78
ρ_2/ρ_1	1.850	1.852
T_2/T_1	13.33	13.80
a_3 (m/s)	1201.1	1206.2
P_3 (MPa)	1.225	1.242
T_3 (K)	3608.3	3603.0
ρ_3	0.9584	0.9726

11 Summary

A series of tests were carried out to generate data that can be used to validate the CV-burn model and Euler equation simulation of detonation propagation. The motivation is to validate the fluid mechanical model that is being used in fluid-structure interaction simulations carried out with the Virtual Test Facility in Caltech's ASC Center. Preliminary experiments identified a number of issues with the experiments and simulations in 2005. A second round of experiments and simulations were carried out in 2006 and significant improvement in the comparison was demonstrated. Some systematic differences in simulations and measured quantities remain, particularly in the long-time reflected waves. Several simulation and experimental issues are offered as explaining the residual differences. Ideal detonation theory and an approximate relationship for the Taylor wave following a detonation were compared to the measured pressures. By adjusting the peak and plateau pressures, a reasonable fit can be obtained and used as a loading function for structural analysis.

12 Acknowledgement

The ASC Center for Simulation of Dynamic Response of Materials is based at the California Institute of Technology and operated under U. S. Department of Energy contract W-7405-ENG-48. We thank Dan Meiron for his leadership and support of these validation activities.

Bibliography

J.B. Bdzil, D. S. Stewart, and T. L. Jackson. Program burn algorithms based on detonation shock dynamics: Discrete approximations of detonation flows with discontinuous front models. *Journal of Computational Physics*, 174:870–902, 2001. 15

W. M. Beltman and J. E. Shepherd. Structural response of shells to detonation and shock loading. Technical report, Graduate Aeronautical Laboratories, California Insititute of Technology, 1998. 5

W.M. Beltman and J.E. Shepherd. Linear elastic response of tubes to internal detonation loading. *Journal of Sound and Vibration*, 252(4):617–655, 2002. 5, 11, 28

W.M. Beltman, E.N. Burcsu, J.E. Shepherd, and L. Zuhal. The structural response of cylindrical shells to internal shock loading. *Journal of Pressure Vessel Technology*, 121: 315–322, 1999. 5

S. Browne, J. Ziegler, and J. E. Shepherd. Numerical solution methods for shock and detonation jump conditions. Technical Report FM2006.006, GALCIT, 2004. 14, 18, 23, 56

T. W. Chao. *Gaseous detonation-driven fracture of tubes*. PhD thesis, California Institute of Technology, 2004. 5

T. W. Chao and J. E. Shepherd. Fracture response of externally flawed aluminum cylindrical shells under internal gaseous detonation loading. *International Journal of Fracture*, 134 (1):59–90, 2005a. 5

T. W. Chao and J. E. Shepherd. Comparison of fracture response of preflawed tubes under internal static and detonation loading. *Journal of Pressure Vessel Technology*, 126(3): 345–353, 2004. 5

T. W. Chao and J. E. Shepherd. Detonation loading of tubes in the modified shear wave regime. In Z. Jiang, editor, *Proceedings of the 24th International Symposium on Shock Waves, volume 2*, pages 865–870. Springer, 2005b. 5

G. Ciccarelli and S. Dorofeev. Flame acceleration and transition to detonation in ducts. *Progress in Energy and Combustion Science*, 2008. in press. 13

F. Cirak, R. Deiterding, and S. P. Mauch. Large-scale fluid-structure interaction simulation of viscoplastic and fracturing thin shells subjected to shocks and detonations. *Computers & Structures*, 85:1049–1065, 2006. 5

R. Deiterding, F. Cirak, S. Mauch, and D. Meiron. A virtual test facility for simulating detonation-induced fracture of thin flexible shells. In V. N. Alexandrov et al., editor, *Proc. Int. Conf. on Comp. Science, May 28-31, 2006, University of Reading*, number 3992 in Lecture Notes in Computer Science, pages 122–130. Springer, Berlin, 2006a. 5, 15

R. Deiterding, R. Radovitzky, S. Mauch, Ludovic Noels, Julian C. Cummings, and Daniel I. Meiron. A virtual test facility for the efficient simulation of solid material response under strong shock and detonation wave loading. *Engineering with Computers*, 22(3-4):325–347, 2006b. 5, 15

R. Deiterding, F.Cirak, S. Mauch, and D. Meiron. A virtual test facility for simulating detonation-induced fracture of thin flexible shells. *Int. J. Multiscale Computational Engineering*, 5(1):47–63, 2007. 5, 15

W. Fickett and W. C. Davis. *Detonation*. University of California Press, Berkerely, CA, 1979. 18, 20

M. Kaneshige and J. E. Shepherd. Detonation database. Technical Report FM97-8, Graduate Aeronautical Laboratories, California Institute of Technology, 1997. See website for most recent update. 7

M. Radulescu and R. K. Hanson. Effect of heat loss on pulse detonation flow fields and performance. *Journal of Propulsion and Power*, 21(2):275–285, 2005. 15

J. E. Shepherd, J. Karnesky, F. Pintgen, and J. C. Krok. Experimental measurements of strains and blast waves resulting from detonations in tubes. Technical Report FM2006.010, Graduate Aeronautical Laboratories, California Institute of Technology, 2008. 5

J.E. Shepherd, A. Teodorcyzk, R. Knystautas, and J.H. Lee. Shock waves produced by reflected detonations. *Progress in Astronautics and Aeronautics*, 134:244–264, 1991. 15

G. I. Taylor. The dynamics of the combustion products behind plane and spherical detonation fronts in explosives. *Proc. Roy. Soc.*, A200:235–247, 1950. 18, 25

P. A. Thompson. *Compressible Fluid Dynamics*. McGraw-Hill, New York, 1972. Out of print from McGraw-Hill, but reprinted privately and available from the Rensselaer Union Bookstore, RPI, Troy, NY. TEL 518 276 6555. 19, 20, 21, 25, 26

E. Wintenberger, J. M. Austin, M. Cooper, S. Jackson, and J. E. Shepherd. Reply to 'comment on analytical model for the impulse of single-cycle pulse detonation tube'. *Journal of Propulsion and Power*, 20(5):957–959, 2004. 15

Ya. B. Zel'dovich and A. S. Kompaneets. *Theory of Detonation*. Academic Press, NY, 1960. English translation of original Russian. 18, 25

A Pressure histories for shots 30-34 in 2005

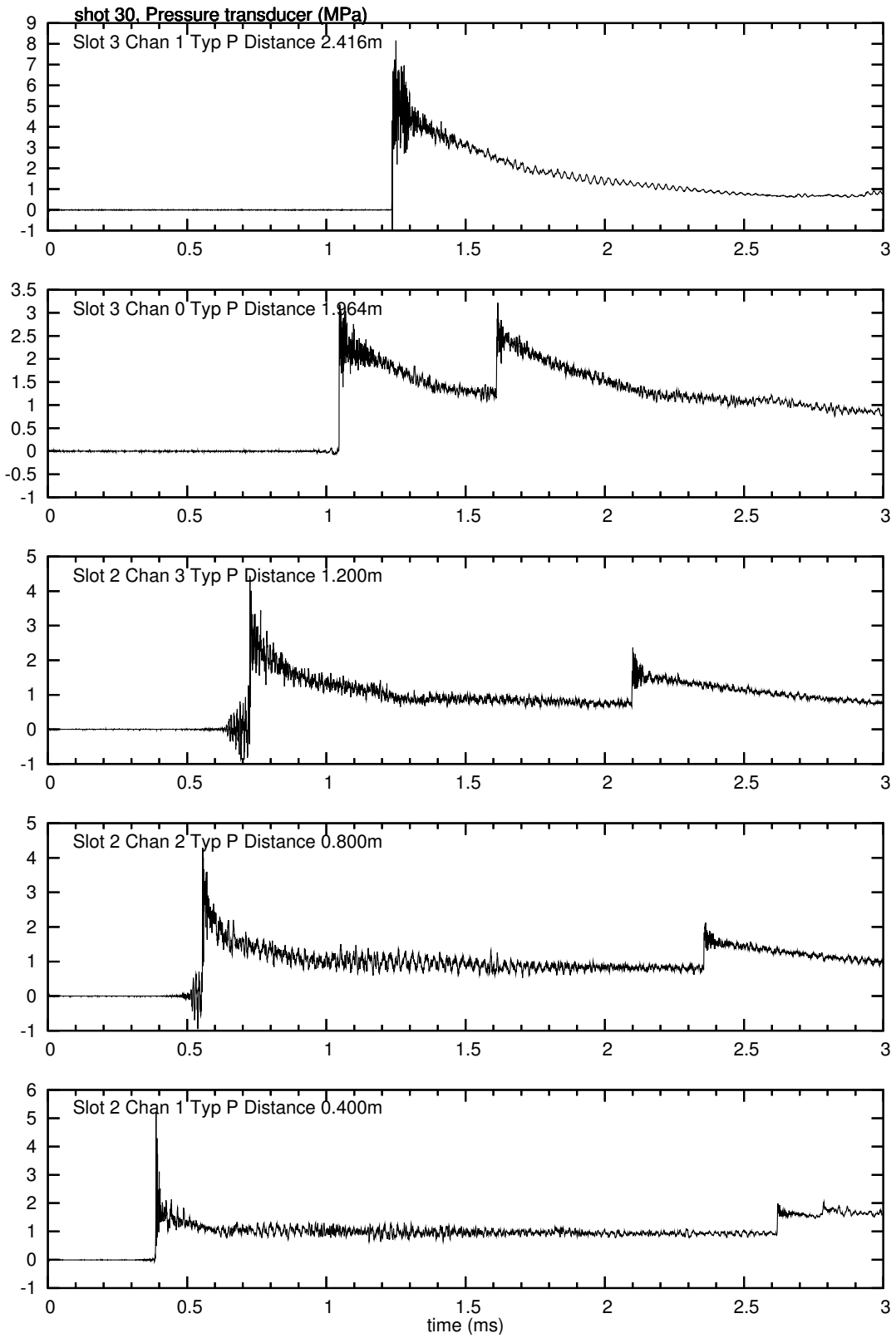

Figure 13: Pressure signals of shot 30 with a short time scale.

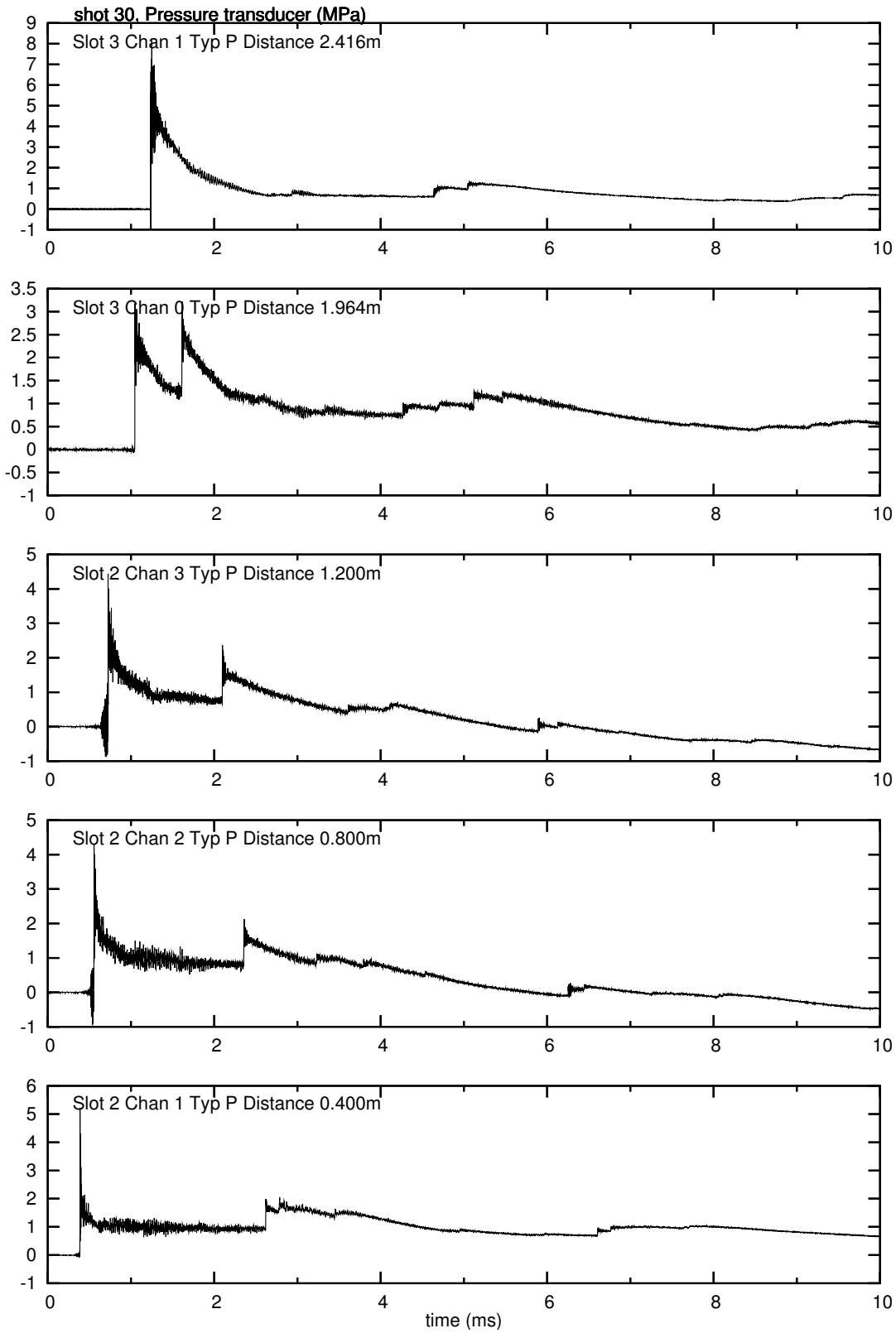

Figure 14: Pressure signals of shot 30.

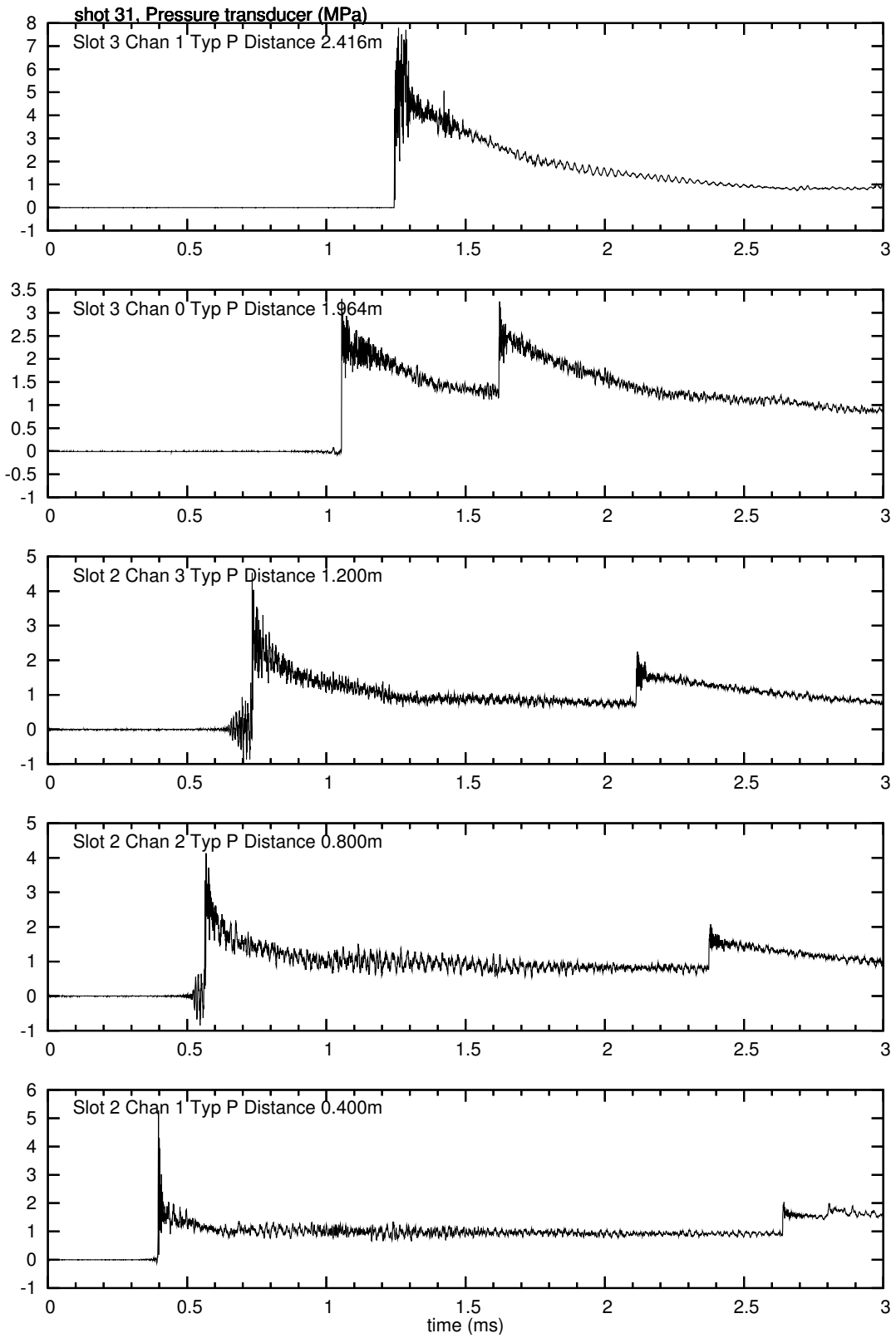

Figure 15: Pressure signals of shot 31 with a short time scale.

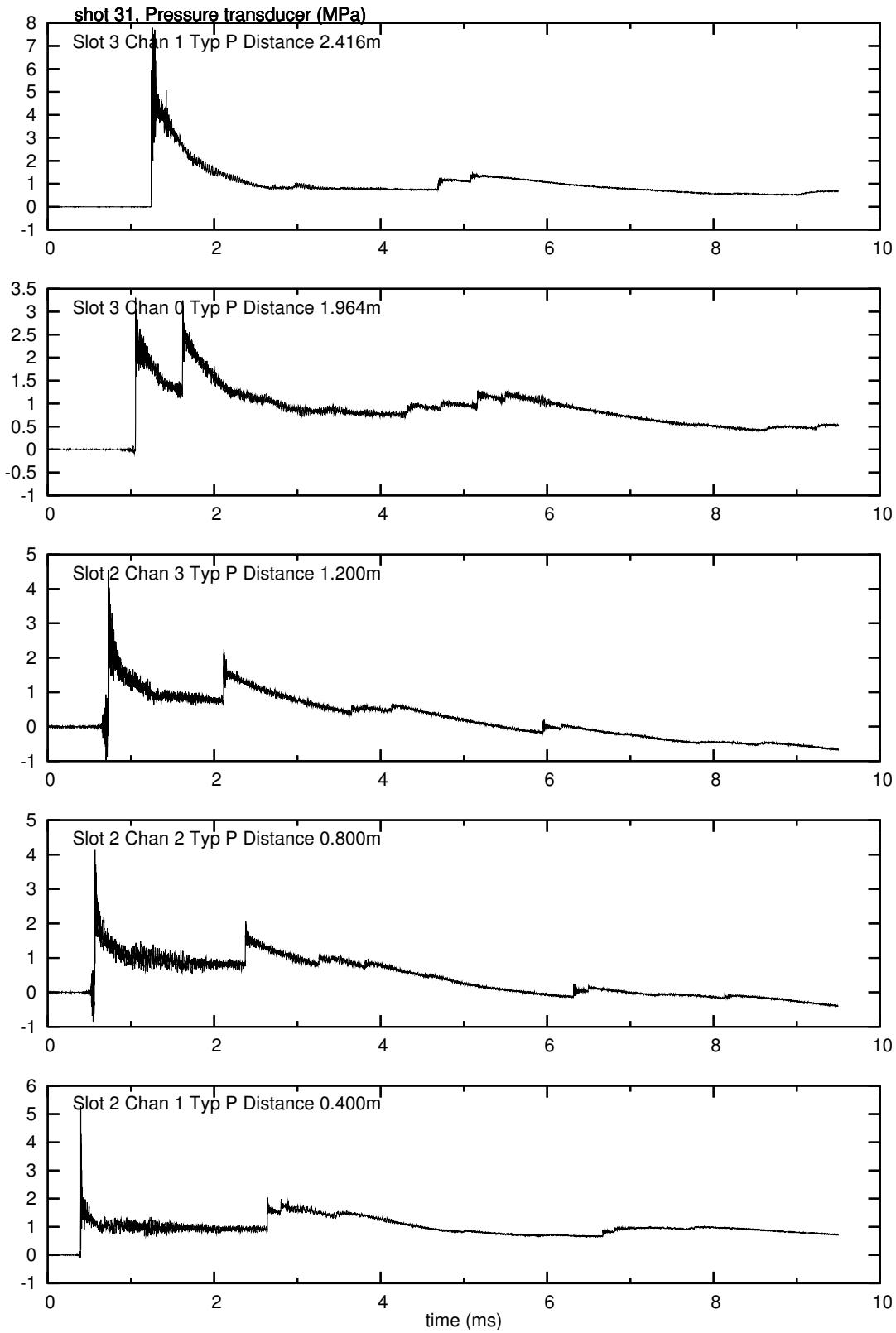

Figure 16: Pressure signals of shot 31.

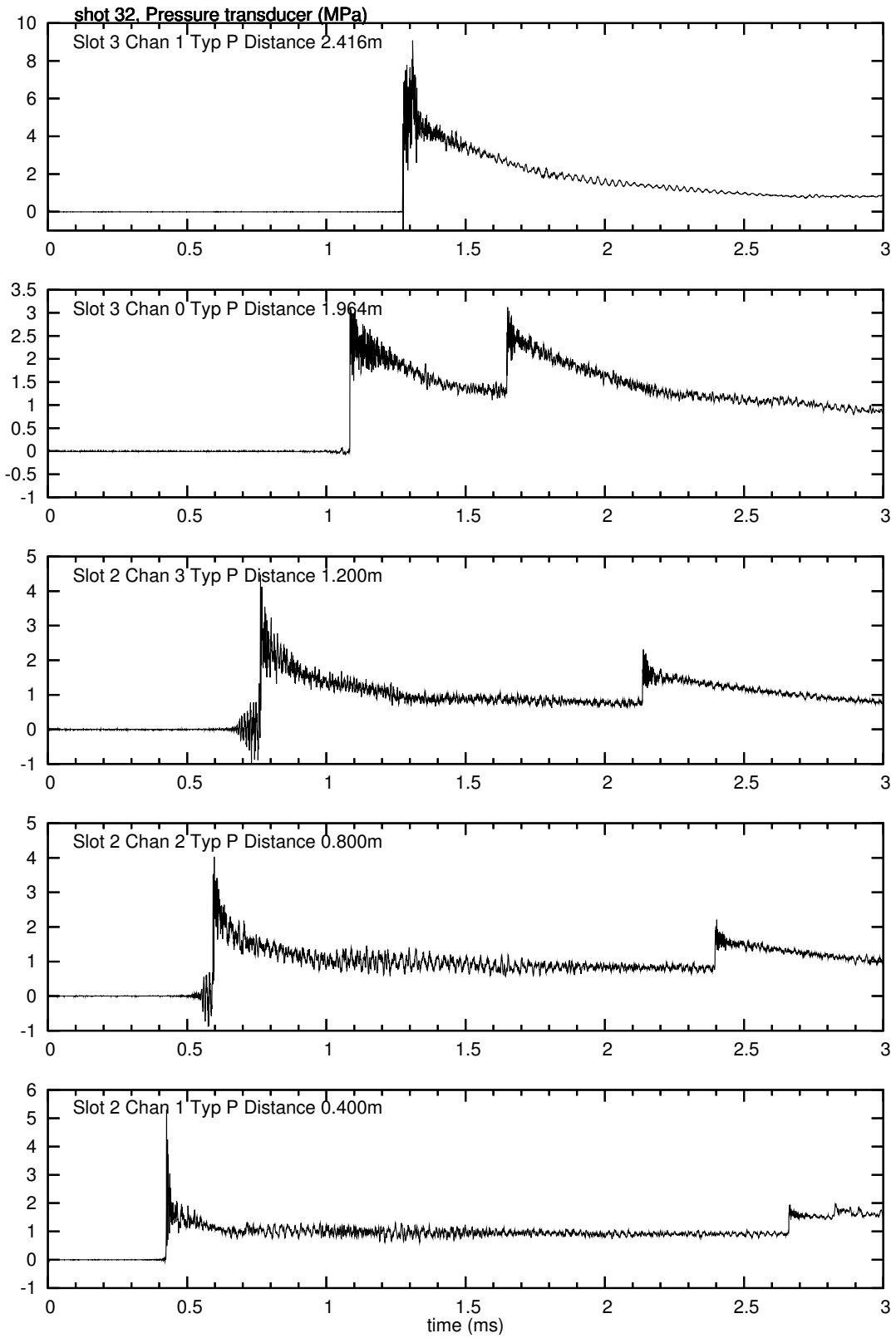

Figure 17: Pressure signals of shot 32 with a short time scale.

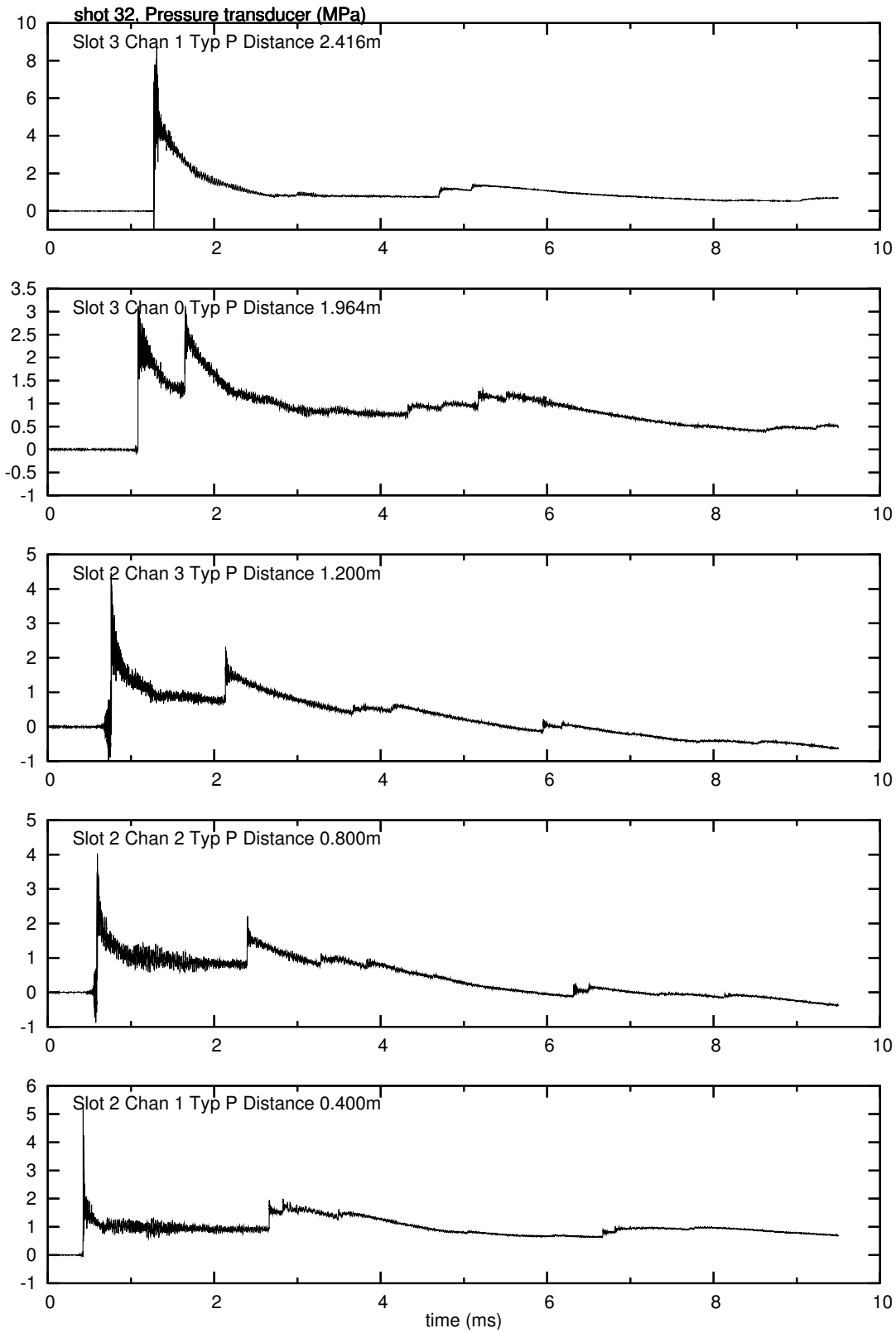

Figure 18: Pressure signals of shot 32.

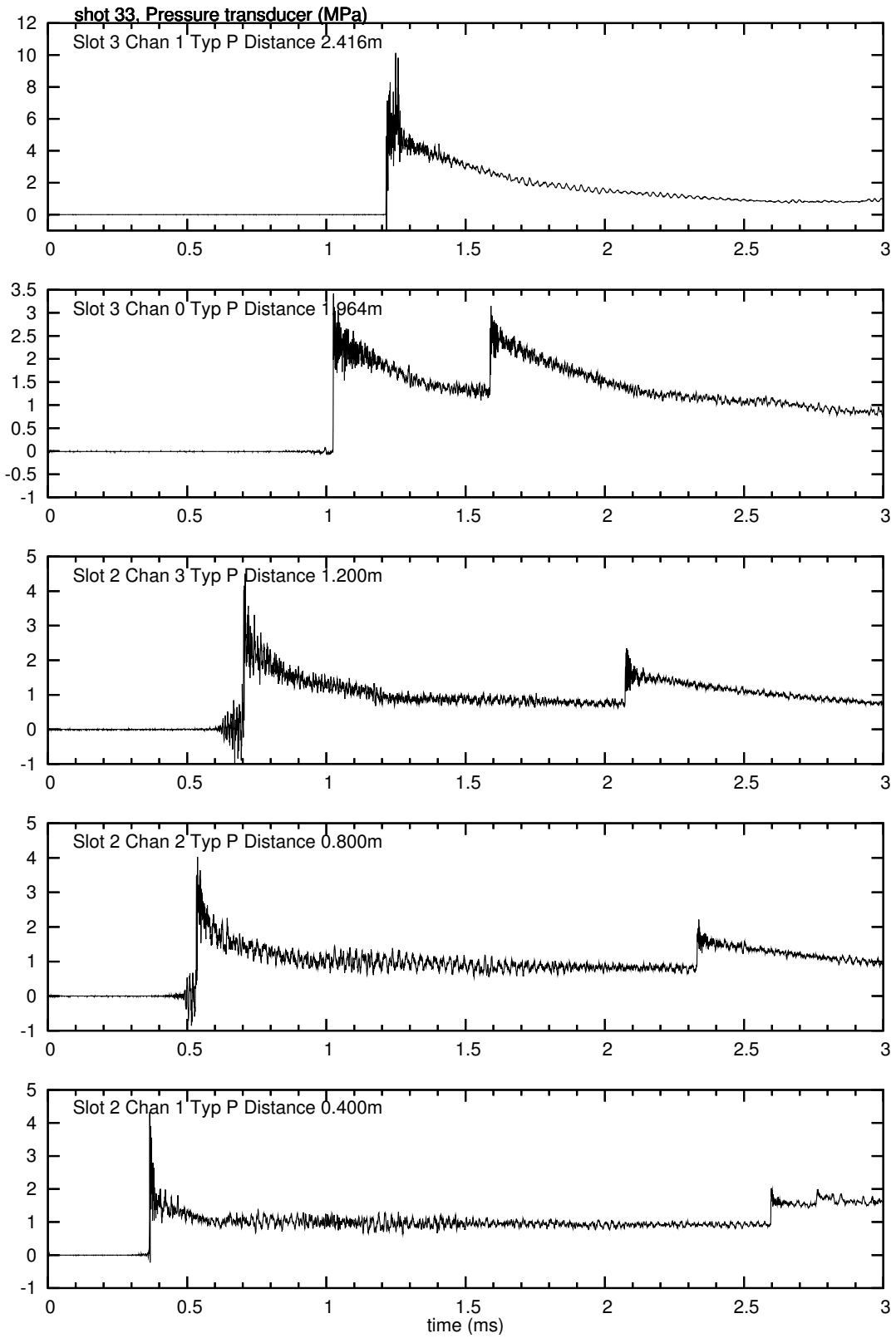

Figure 19: Pressure signals of shot 33 with a short time scale.

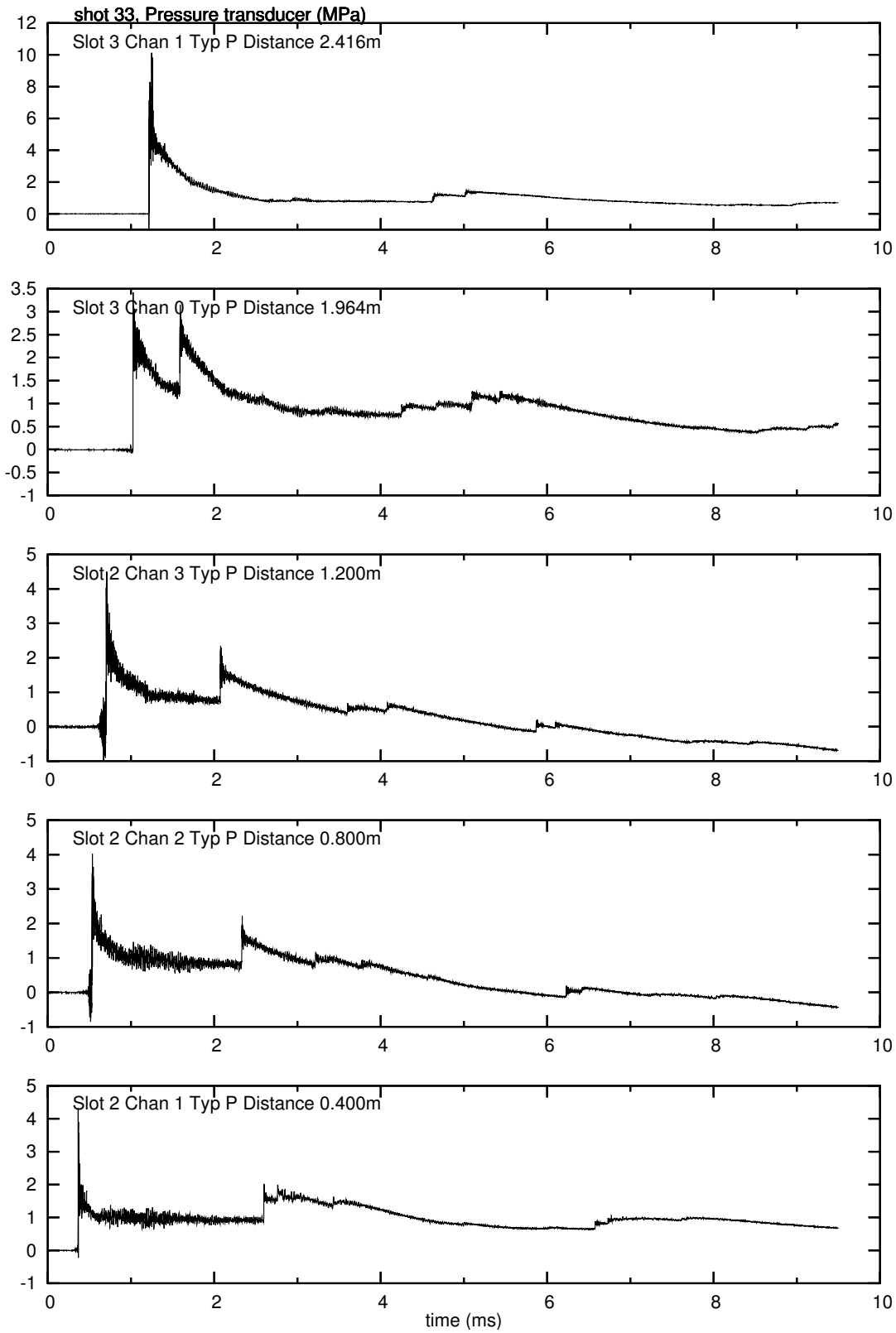

Figure 20: Pressure signals of shot 33.

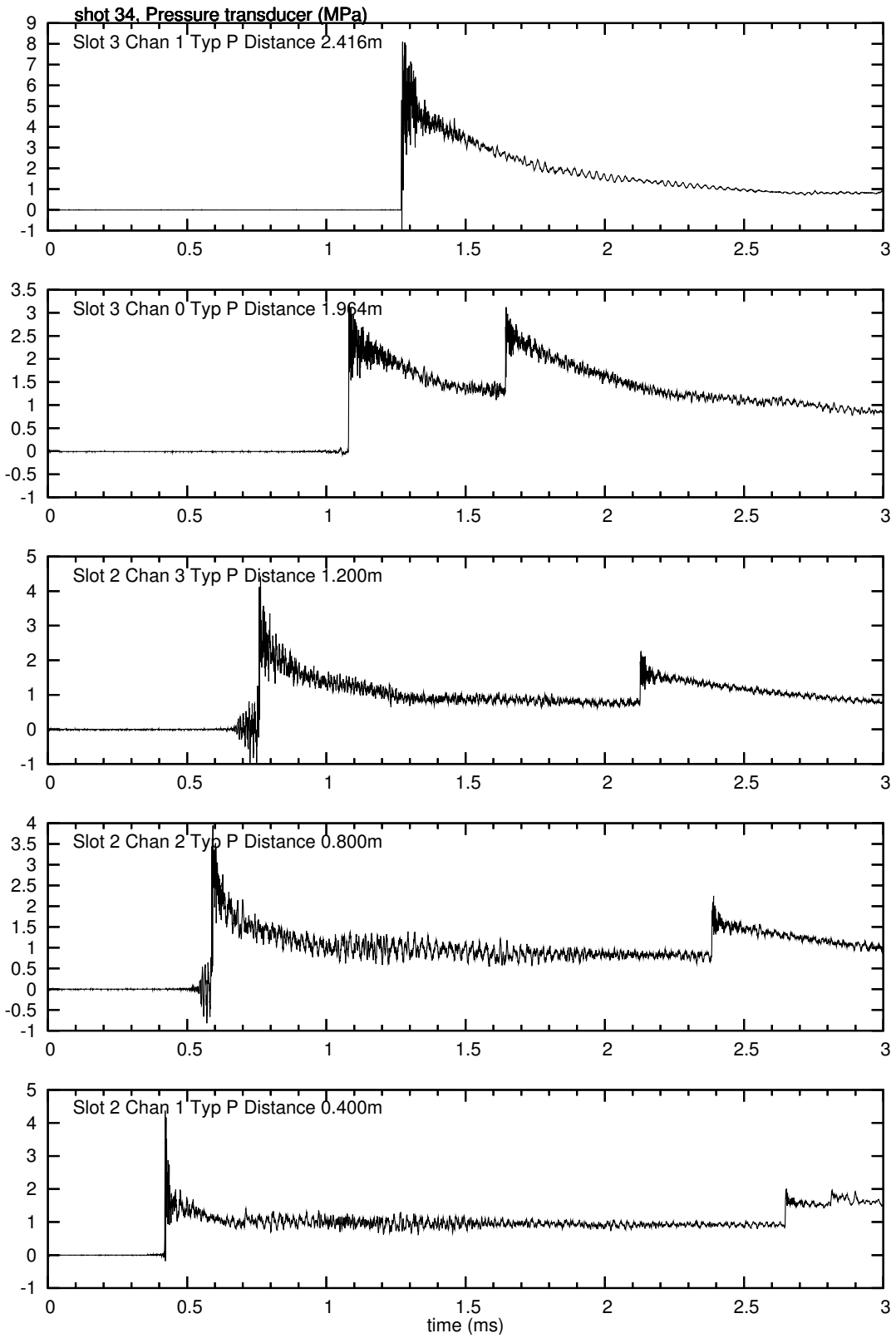

Figure 21: Pressure signals of shot 34 with a short time scale.

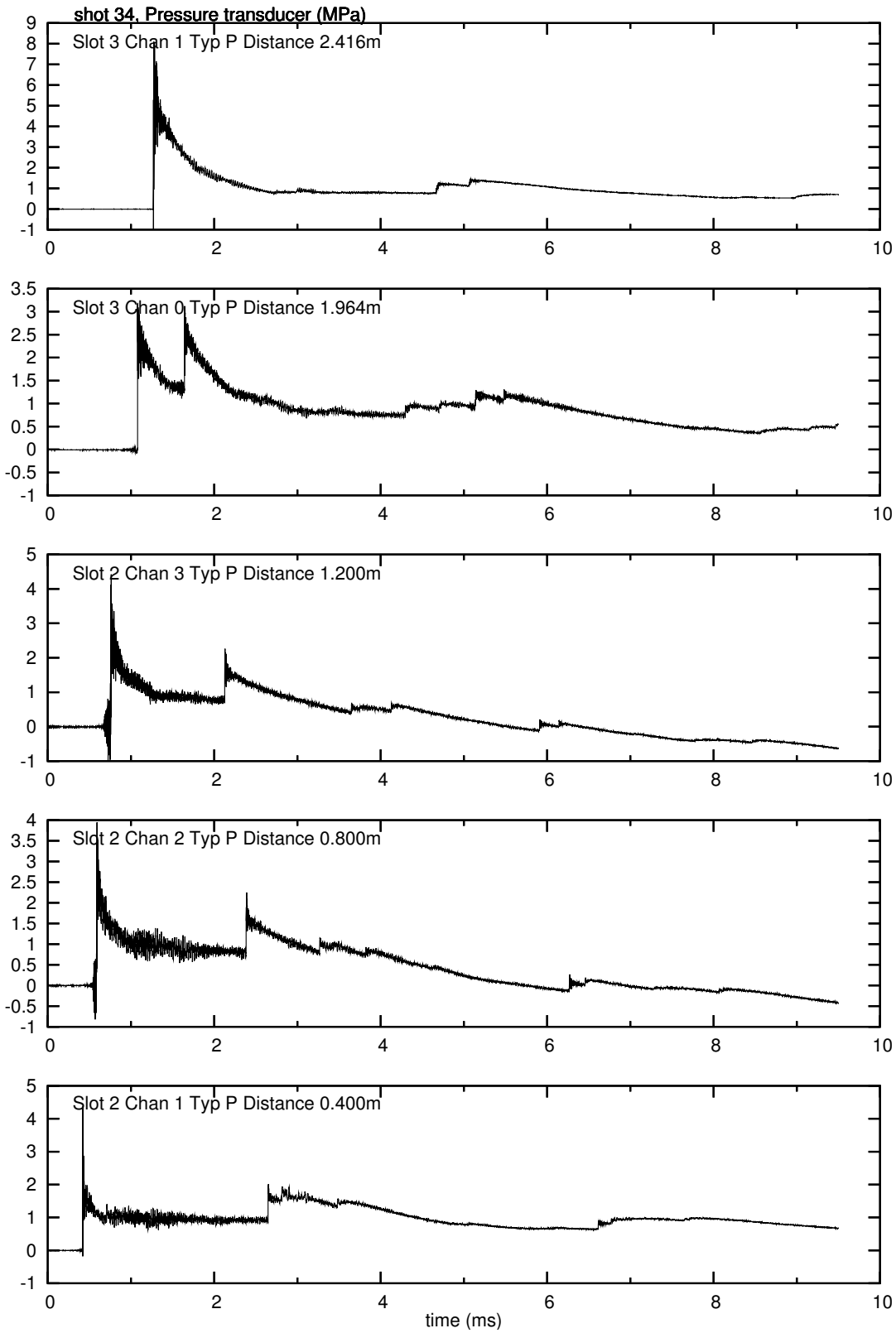

Figure 22: Pressure signals of shot 34.

B Pressure histories for shots 1-7 in 2006

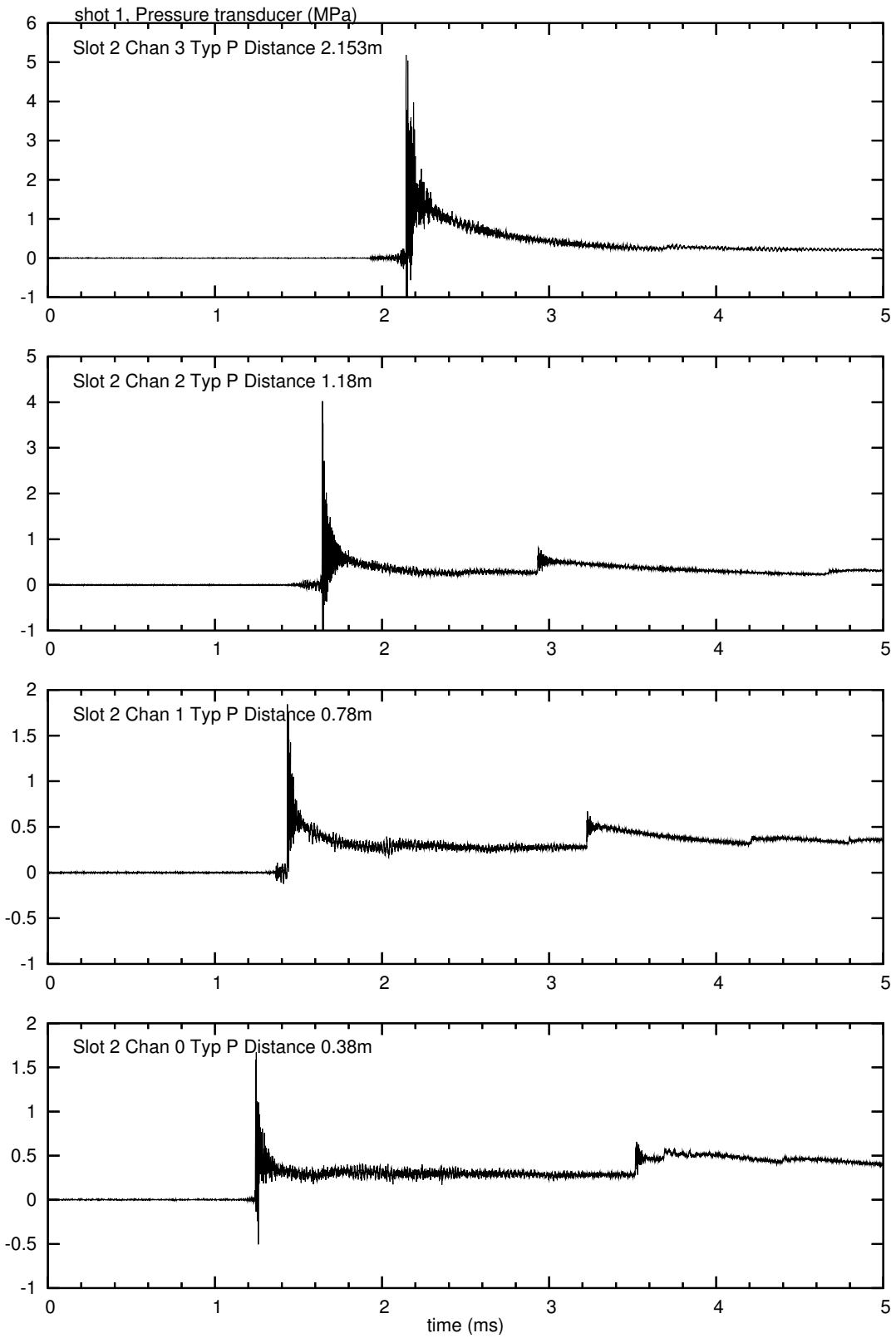

Figure 23: Pressure signals of shot 1 with a short time scale.

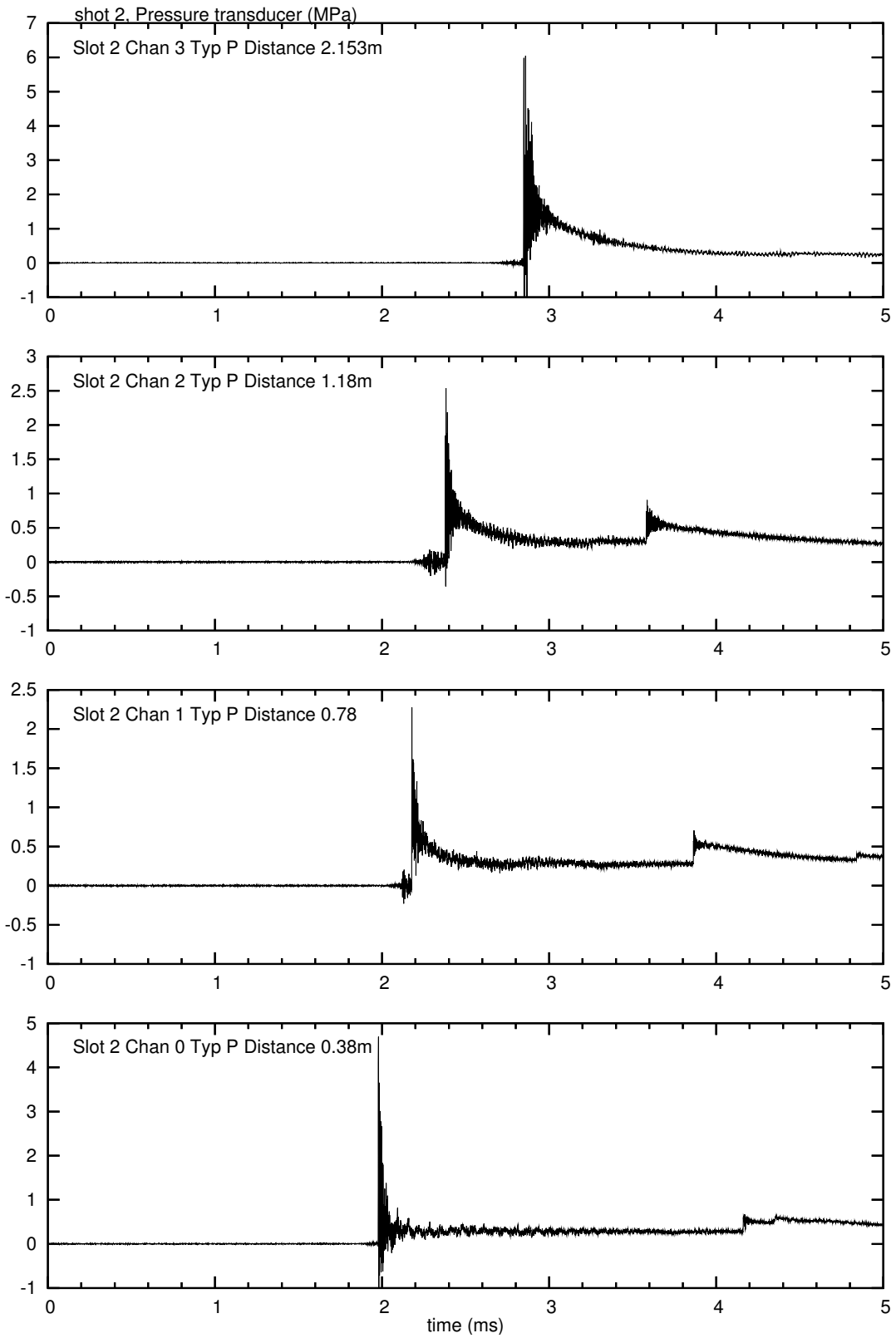

Figure 24: Pressure signals of shot 2 with a short time scale.

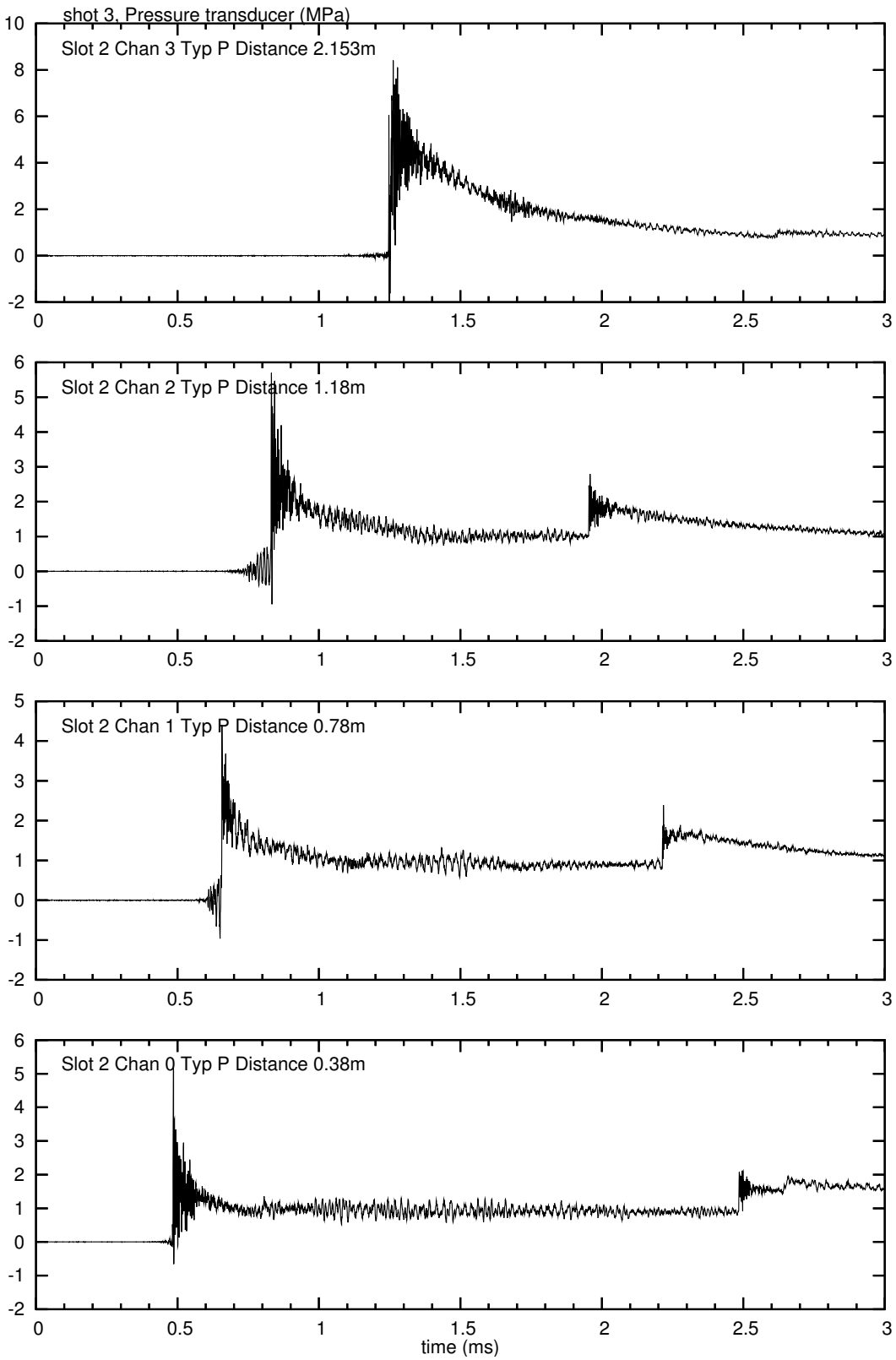

Figure 25: Pressure signals of shot 3 with a short time scale.

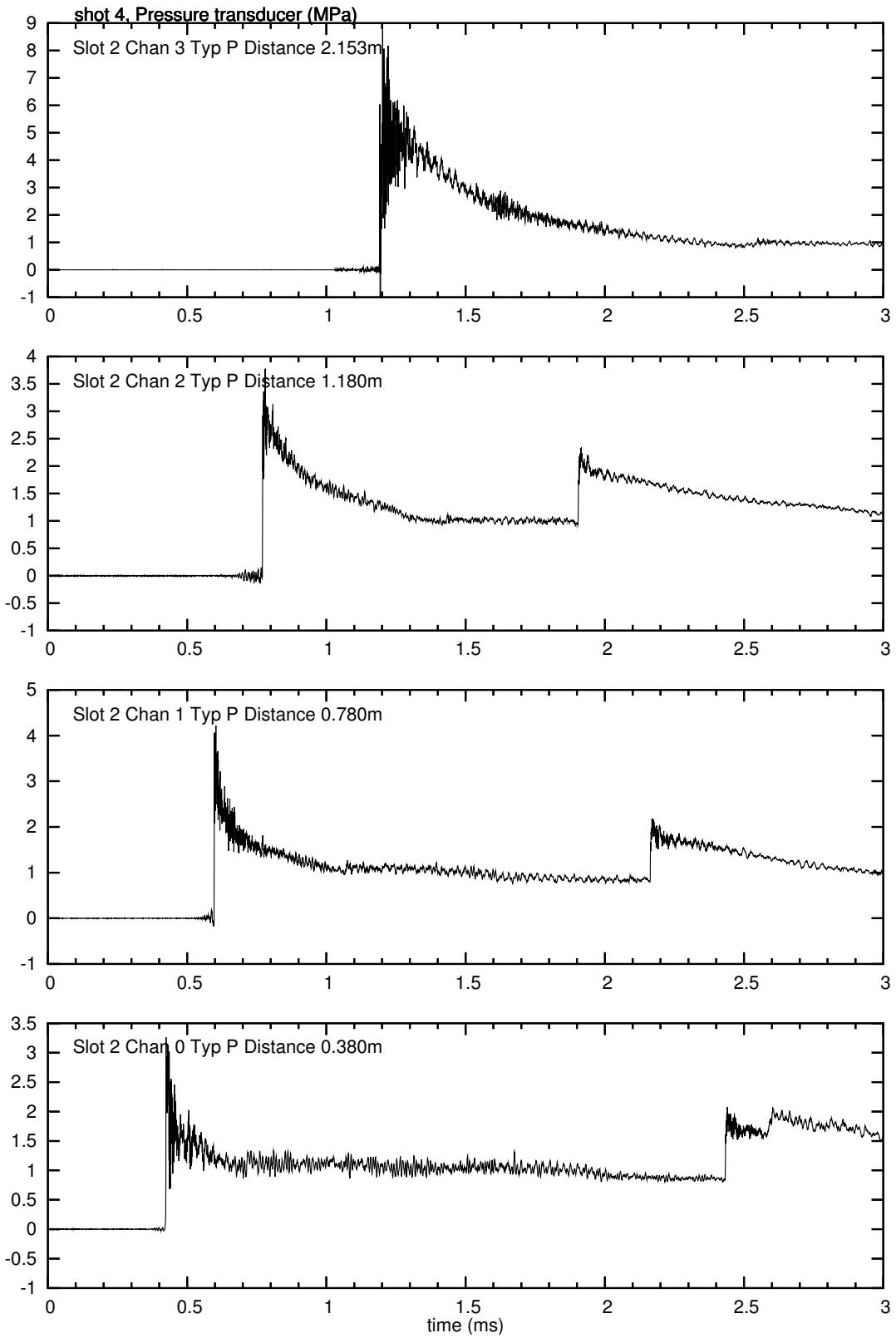

Figure 26: Pressure signals of shot 4 with a short time scale.

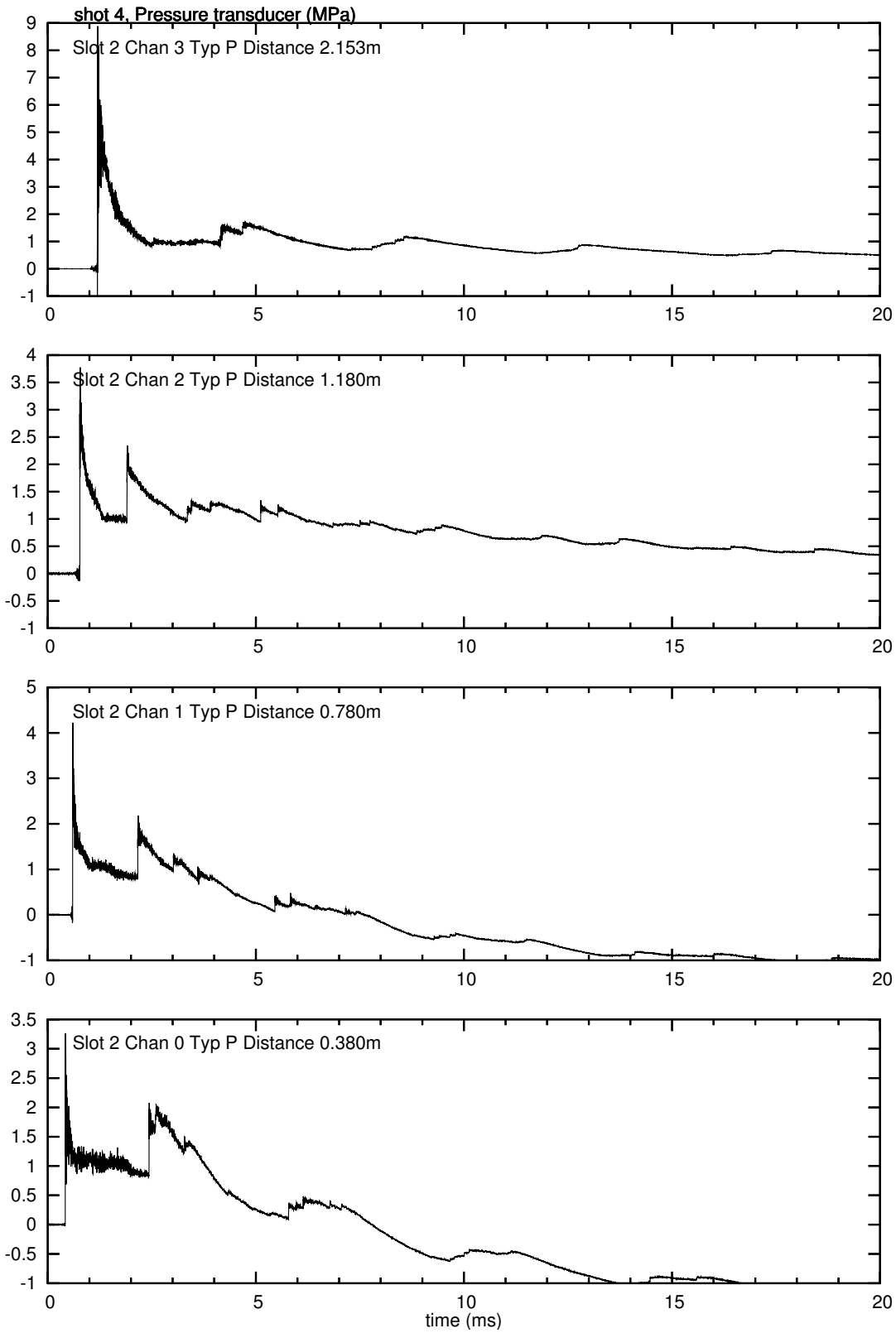

Figure 27: Pressure signals of shot 4.

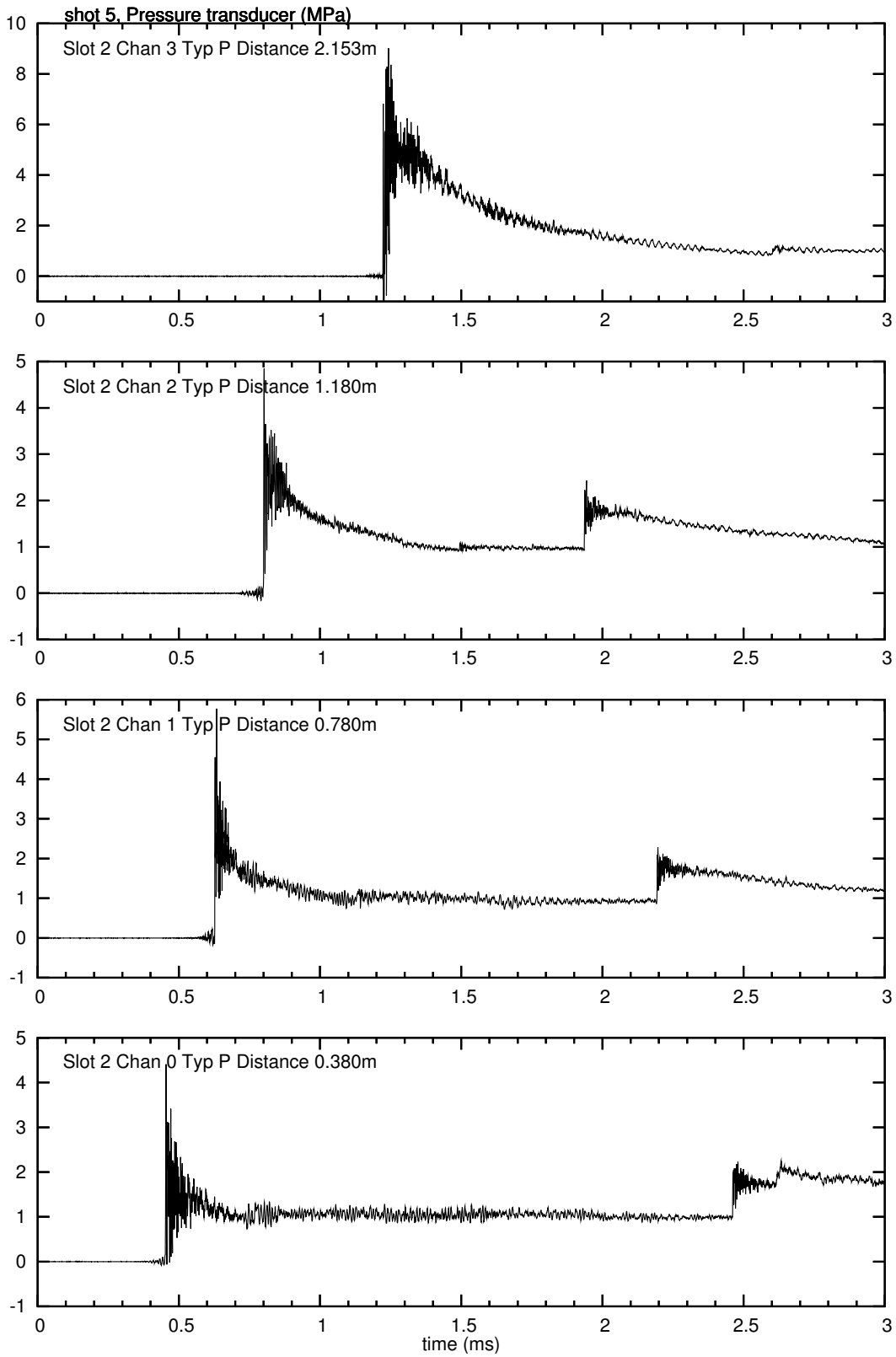

Figure 28: Pressure signals of shot 5 with a short time scale.

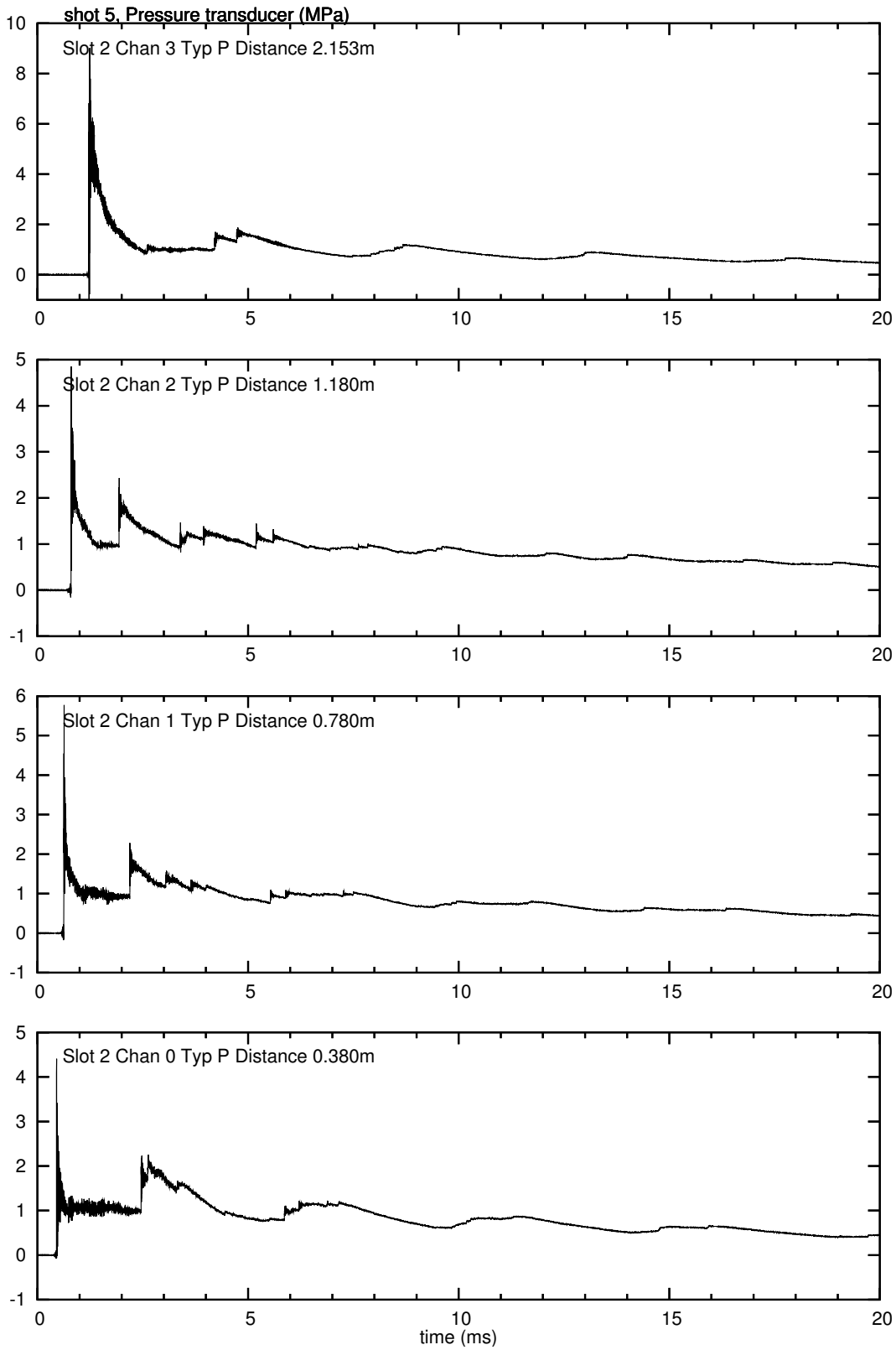

Figure 29: Pressure signals of shot 5.

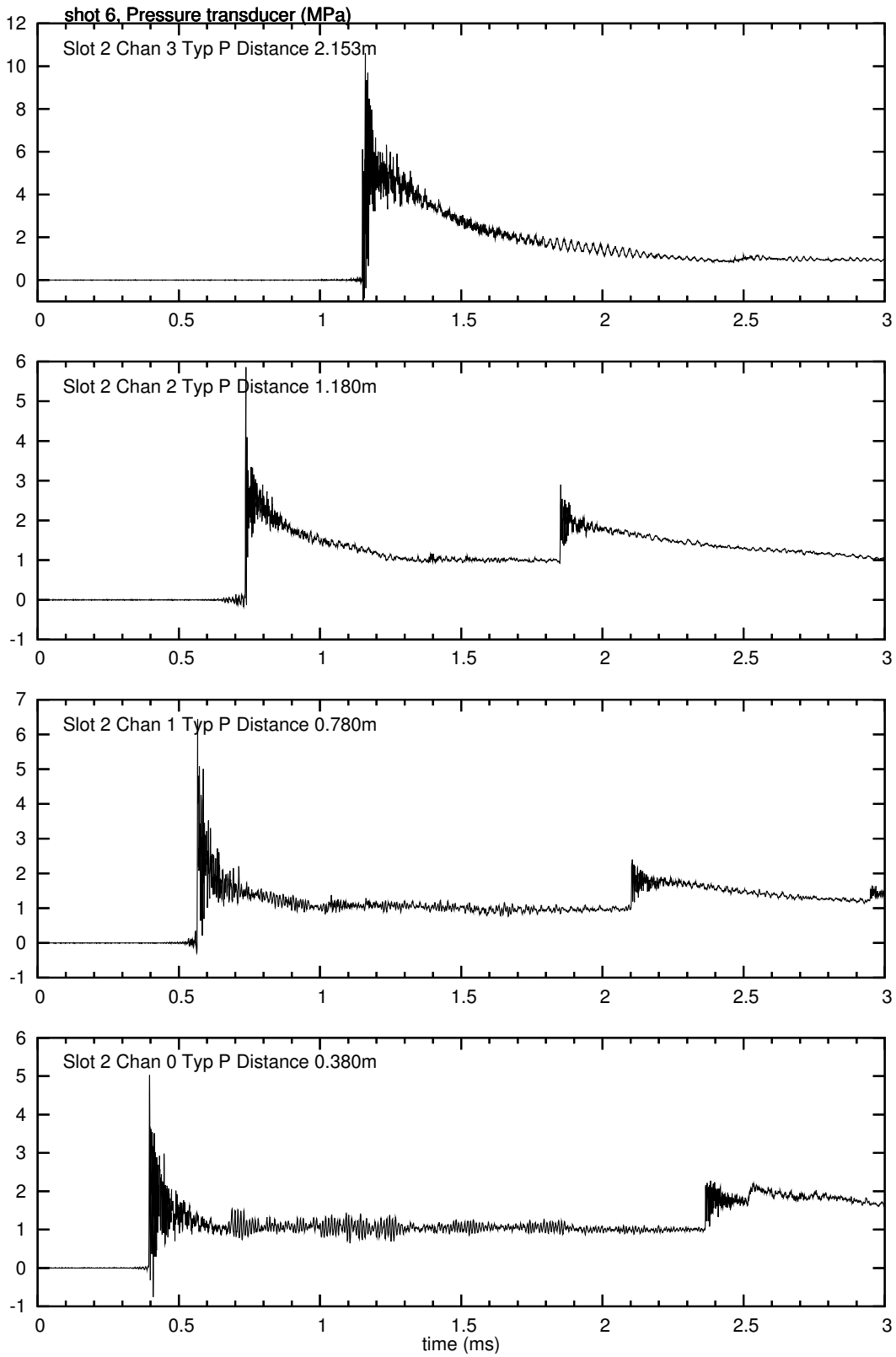

Figure 30: Pressure signals of shot 6 with a short time scale.

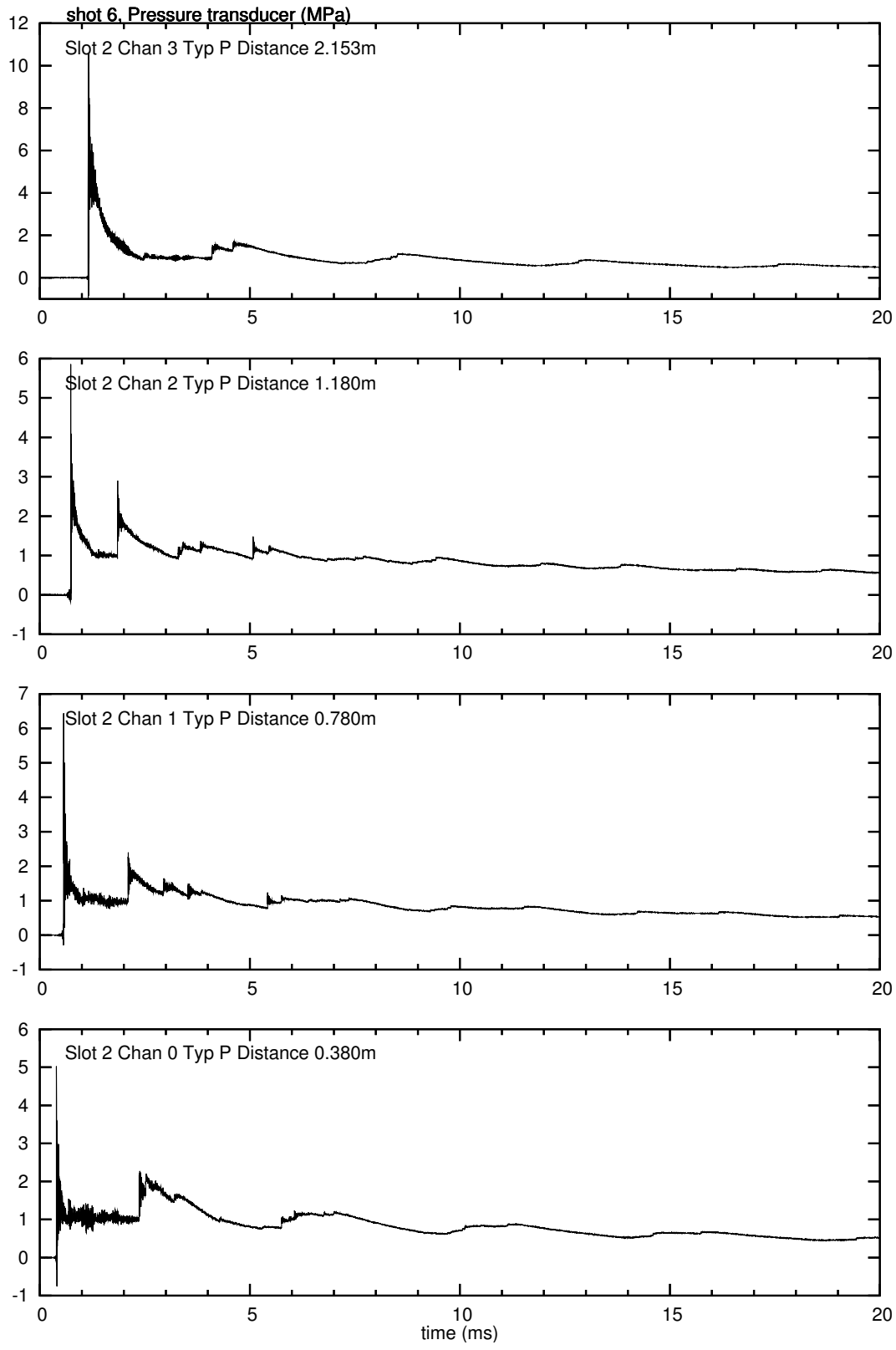

Figure 31: Pressure signals of shot 6.

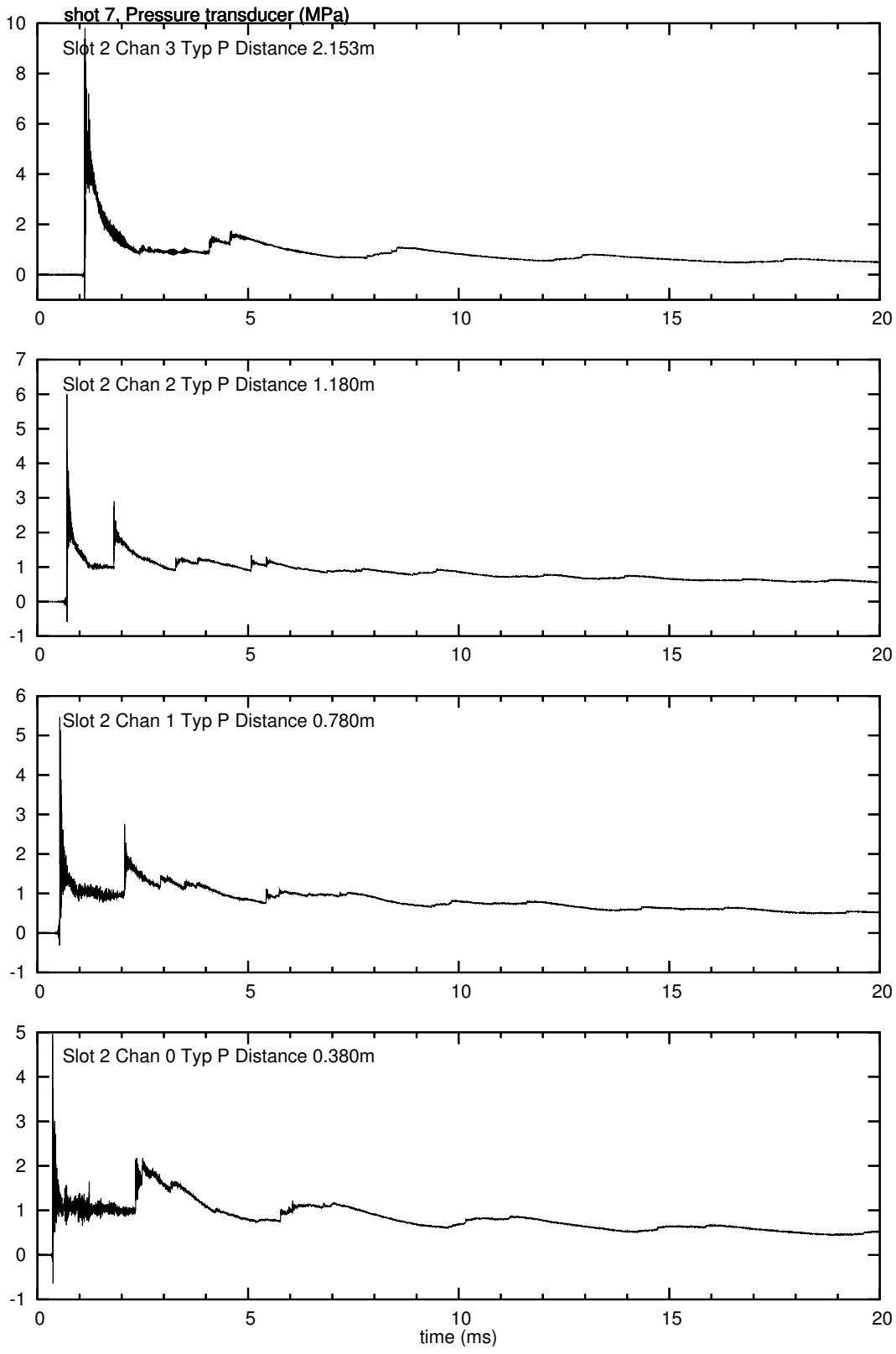

Figure 32: Pressure signals of shot 7.

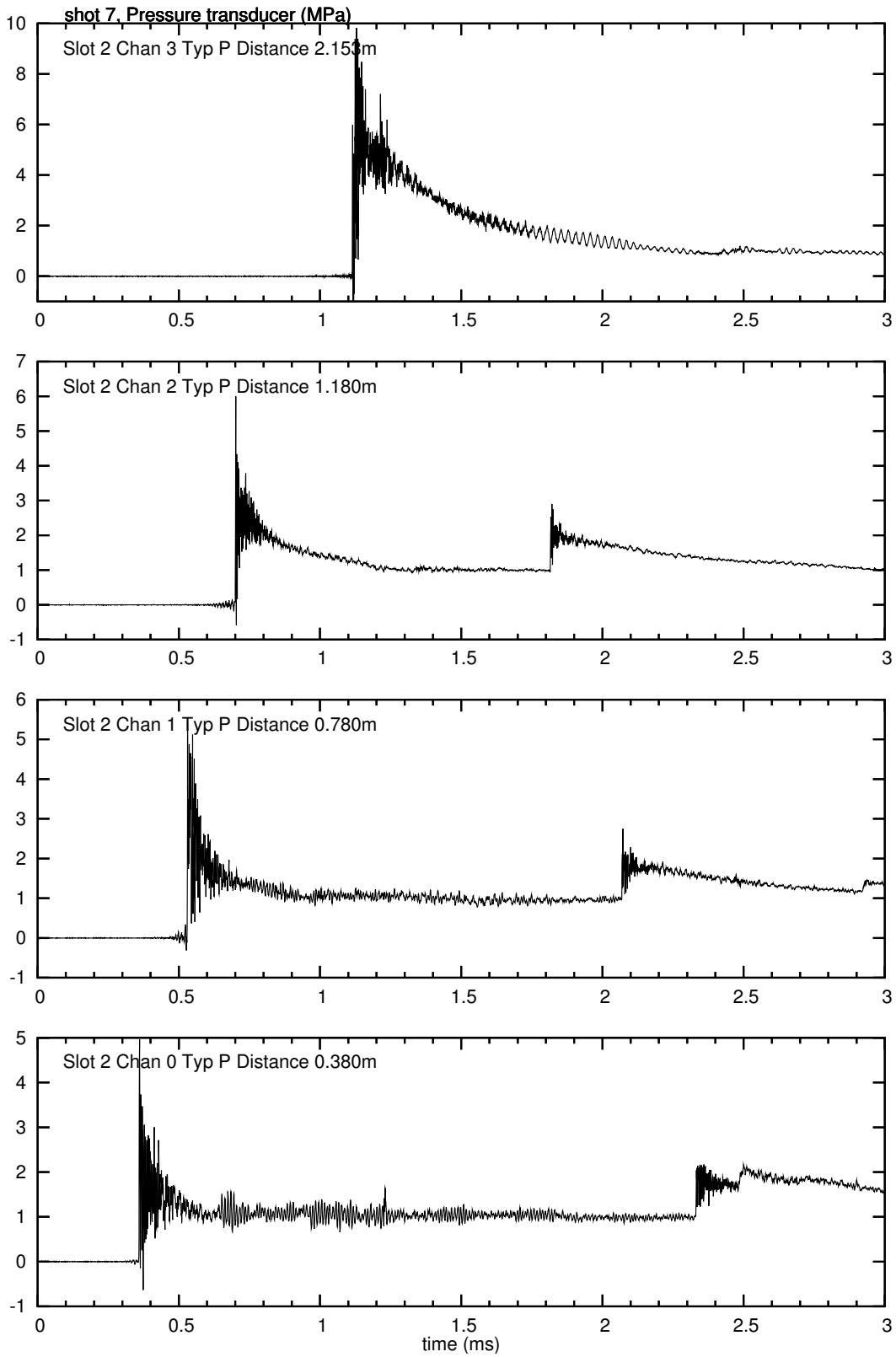

Figure 33: Pressure signals of shot 7 with a short time scale.

C Computed CJ and Isentrope States

The CJ state and isentrope in the products was computed using the `demo_CJState-isentrope.m` program of the Shock and Detonation Toolbox (Browne et al., 2004). The output for the nominal 100 kPa, 296 K initial conditions is given below.

```
Initial pressure 100000 (Pa)
Initial temperature 296 (K)
Initial density 1.2601 (kg/m3)
a1 (frozen) 326.2423 (m/s)
gamma1 (frozen) 1.3412 (m/s)
Computing CJ state and isentrope for C2H4:1 O2:3.001 using gri30_highT.cti
CJ speed 2373.4354 (m/s)
CJ pressure 3361533.9338 (Pa)
CJ temperature 3932.9145 (K)
CJ density 2.3313 (kg/m3)
CJ entropy 11710.4445 (J/kg-K)
w2 (wave frame) 1282.9257 (m/s)
u2 (lab frame) 1090.5097 (m/s)
a2 (frozen) 1335.3324 (m/s)
a2 (equilibrium) 1281.4276 (m/s)
gamma2 (frozen) 1.2366 (m/s)
gamma2 (equilibrium) 1.1388 (m/s)
Detonation CJ Mach number) 7.2751 (m/s)
2-gamma energy parameter q 9526253.129 (J/kg)
Generating points on isentrope and computing Taylor wave velocity
State 3 pressure 1222649.2705 (Pa)
State 3 temperature 3608.6255 (K)
State 3 volume 1.0471 (m3/kg)
State 3 sound speed (frozen) 1254.4746 (m/s)
State 3 sound speed (equilibrium) 1201.7509 (m/s)
State 3 gamma frozen) 1.2292 (m/s)
State 3 gamma (equilibrium) 1.1281 (m/s)
```

D Modified Fixture Engineering Drawings

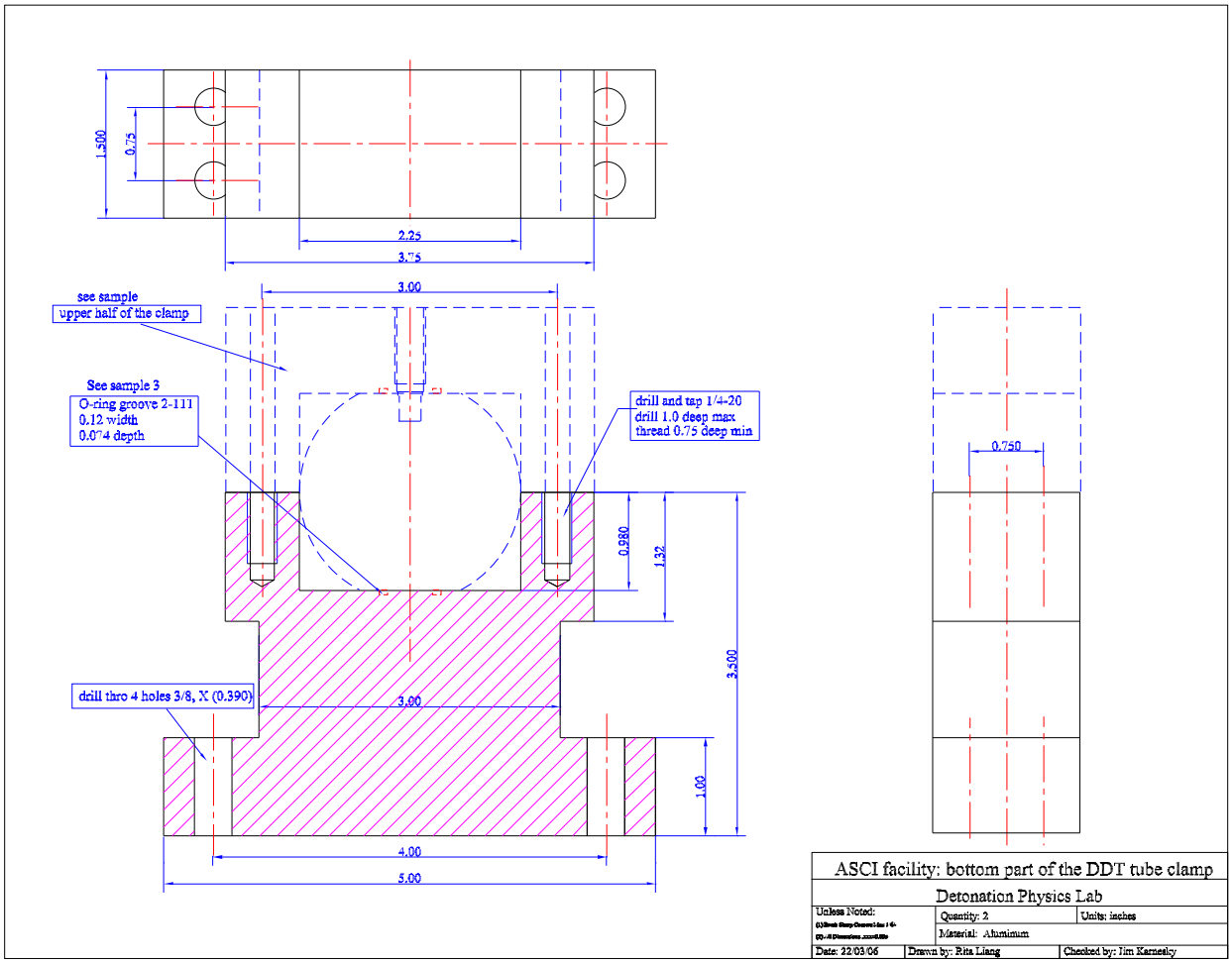

Figure 34: Modified clamp.

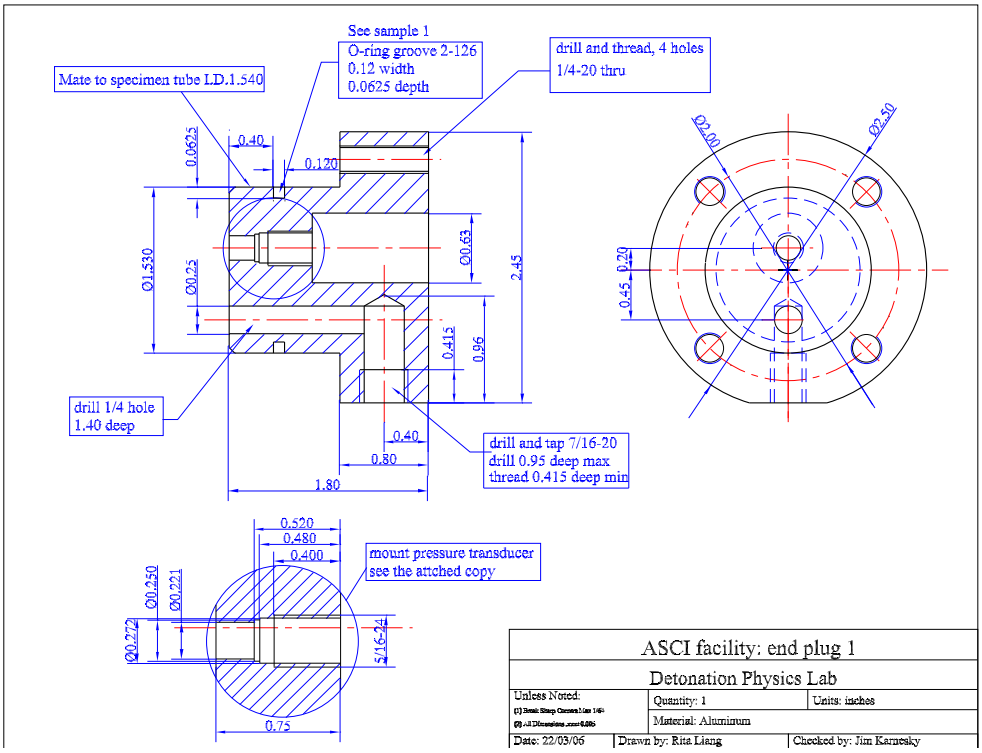

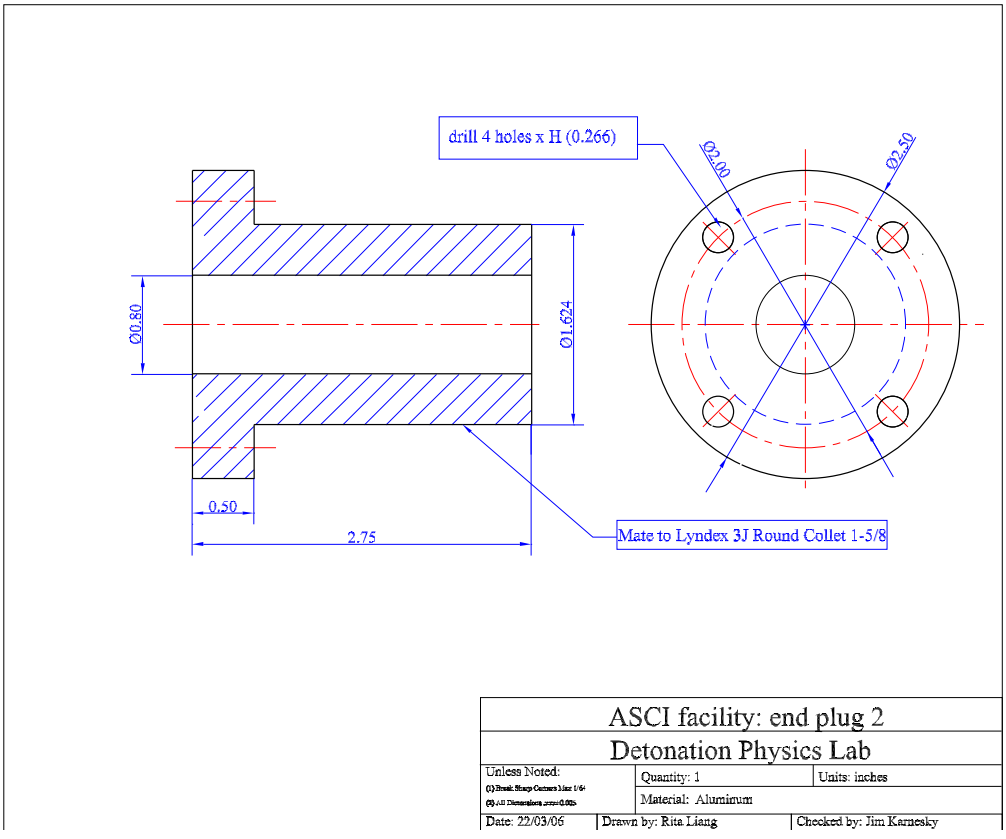

Figure 35: Modified end plugs.